DUAL ENCAPSULATION OF GOLD NANORODS AND CHEMOTHERAPY DRUGS INTO PLGA NANOPARTICLES FOR COMBINED CANCER THERAPY

by

İrem Sultan İlçi

B.S., in Bioengineering, Yıldız Technical University, 2021

Submitted to the Institute of Biomedical Engineering
in partial fulfillment of the requirements
for the degree of
Master of Science
in
Biomedical Engineering

Boğaziçi University
2025

DUAL ENCAPSULATION OF GOLD NANORODS AND CHEMOTHERAPY DRUGS INTO PLGA NANOPARTICLES FOR COMBINED CANCER THERAPY

APPROVED BY:

Assoc. Prof. Dr. Banu İyisan (Thesis Advisor)	.....
Prof. Dr. Bora Garipcan	.....
Assist. Prof. Dr. Z. Cansu Canbek Özdil	.....

DATE OF APPROVAL: 21.08.2025

ACKNOWLEDGMENTS

This thesis marks the end of a long and transformative journey, during which I not only gained technical knowledge, but also grew through moments of doubt, resilience, and reflection.

First and foremost, I would like to express my sincere gratitude to my advisor, Assoc. Prof. Banu İyisan for her invaluable guidance, patience, and unwavering support. Through her mentorship, I learned how to express my ideas clearly, ask the right questions, and most importantly, to think independently and critically. Her encouragement made it easier to navigate uncertainty, and her trust helped me grow beyond my own expectations.

I would also like to thank my Bindlab mates, whose presence made this journey less isolating and much more meaningful. Our discussions, scientific or otherwise, challenged me, encouraged me, and often reminded me that growth is rarely linear. I am especially grateful for the shared moments of struggle and support that shaped not only the outcome of this thesis, but also my understanding of collaboration and empathy.

To my friends and family, thank you for your quiet strength and for giving me the space to fall and rise again and I am thankful for your love, even when you did not always understand what I was going through. And finally, I dedicate this thesis to the version of myself who kept going even when she was tired, who chose to show up despite the fear, and who, through every setback, refused to give up.

This study was fully supported by the Scientific&Technological Research Council of Turkey (TÜBİTAK) (Project Number 121C205) and Max Planck Society through Max Planck Partner Groups Grant.

ACADEMIC ETHICS AND INTEGRITY STATEMENT

I, İrem Sultan İlçi, hereby certify that I am aware of the Academic Ethics and Integrity Policy issued by the Council of Higher Education (YÖK) and I fully acknowledge all the consequences due to its violation by plagiarism or any other way.

Name :

Signature:

Date:

ABSTRACT

DUAL ENCAPSULATION OF GOLD NANORODS AND CHEMOTHERAPY DRUGS INTO PLGA NANOPARTICLES FOR COMBINED CANCER THERAPY

Due to its multifaceted nature, cancer often requires combination therapies for effective treatment. In this study, we report the development of a dual–functional nanoplatform in which gold nanorods (AuNRs) and doxorubicin (DOX) are co–encapsulated within poly(lactic–co–glycolic acid) (PLGA) nanoparticles (≈246 nm). The miniemulsion-based formulation produced nanoparticles with a narrow size distribution (PDI ≤ 0.1), a DOX loading of 32±4 μg/mL, and 47% AuNR encapsulation efficiency. AuNR encapsulated PLGA nanoparticles retained their structural integrity, shape, and longitudinal surface plasmon resonance (LSPR) properties during 110–day storage at 4 °C. Upon near-infrared laser irradiation (808 nm, 1 W/cm^2, 5 min), nanoparticles generated a temperature increase of approximately 25 °C, confirming preserved photothermal performance. 3-(4,5-Dimethylthiazol-2-yl)-2,5-Diphenyltetrazolium Bromide (MTT) assays in MCF–7 breast cancer cells revealed that cytotoxicity was primarily driven by the DOX payload, with no statistically significant synergy observed between chemotherapy and photothermal effects.

Keywords: PLGA Nanoparticles, Gold Nanorods, Doxorubicin, Dual Photothermal–Chemotherapy System, Colloidal Stability, MCF–7 Breast-Cancer Cells.

ÖZET

KOMBİNE KANSER TEDAVİSİ İÇİN ALTIN NANOÇUBUKLARIN VE KEMOTERAPİ İLAÇLARININ PLGA NANOPARTİKÜLLERİNE İKİLİ ENKAPSÜLASYONU

Kanserin çok yönlü yapısı, etkili bir tedavi için genellikle birden fazla yaklaşımın birlikte kullanılmasını gerektirir. Bu çalışmada, altın nanoçubuklar (AuNR) ve doksorubisin (DOX) birlikte poli(laktik-ko-glikolik asit) (PLGA) nanoparçacıklarına enkapsüle edilerek geliştirilen çift işlevli bir nanoplatform sunulmuştur. Geliştirilen nanoparçacıkların ortalama çapı yaklaşık 246 nm'dir. Miniemülsiyon yöntemiyle hazırlanan formülasyon, dar bir boyut dağılımı (PDI $\leq$ 0.1), 32$\pm$4 μg/mL DOX yükleme miktarı ve %47 oranında AuNR enkapsülasyon verimi sağlamıştır. PLGA içine enkapsüle edilen AuNR'lerin yapısal bütünlüğü, şekli ve boylamsal yüzey plazmon rezonansı (LSPR) özellikleri 4 °C'de 110 gün boyunca korunmuştur. Yakın kızılötesi (NIR) lazer (808 nm, 1 W/cm^2, 5 dakika) uygulaması sonucunda,nanoparçacıklar yaklaşık 25 °C'lik bir sıcaklık artışı sağlamıştır. Bu sonuç, sistemin fototermal performansını koruduğunu göstermektedir. MCF-7 meme kanseri hücrelerinde yapılan MTT testi sonuçlarına göre, sitotoksisite büyük ölçüde DOX'un kemoterapötik etkisine bağlıdır. Fototermal etki ile anlamlı bir sinerji gözlemlenmemiştir. Çalışmada elde edilen veriler, AuNR'lerin PLGA içine yüklendiğinde plazmonik özelliklerini koruduğunu göstermektedir.

Anahtar Sözcükler: PLGA Nanoparçacıklar, Altın Nanoçubuklar, Doksorubisin, Kombine Fototermal-Kemoterapi Sistemi, Kolloidal Stabilite, MCF-7 Meme Kanseri Hücreleri.

TABLE OF CONTENTS

LIST OF FIGURES

LIST OF TABLES

LIST OF SYMBOLS

%	Percentage
%wt	Weight percent
°	Degree
°C	Celcius
μg	Microgram
μL	Microliter
kDa	Kilodalton
mg	Mlligram
mL	Milliliter
nm	Nanometer
rpm	Revolutions per minute
v/v	Volume per volume
w/w	Weight per weight
W	Watt
ζ	Zeta potential
λ	Wavelength

LIST OF ABBREVIATIONS

AKT	Protein Kinase B
AuNR	Gold Nanorod
BC	Breast Cancer
BCSC	Breast Cancer Stem Cell
CTAB	Cetyltrimethylammonium Bromide
CW	Continuous Wave
dPBS	Dulbecco's Phosphate–Buffered Saline
DLS	Dynamic Light Scattering
DMEM	Dulbecco's Modified Eagle's Medium
DMSO	Dimethyl Sulfoxide
DOX	Doxorubicin Hydrochloride
EPR	Enhanced Permeability and Retention
ELS	Electrophoretic Light Scattering
FBS	Fetal Bovine Serum
FTIR	Fourier–Transform Infrared Spectroscopy
HSA	Human Serum Albumin
LA	Lactic Acid
LSPR	Longitudinal Surface Plasmon Resonance
MDR	Multidrug Resistance
MRI	Magnetic Resonance Imaging
MTT	3-(4,5-Dimethylthiazol-2-yl)-2,5-Diphenyltetrazolium Bromide
MW	Molecular Weight
NIR	Near-Infrared
NRF2	Nuclear Factor Erythroid 2-Related Factor 2
PCL	Poly(Caprolactone)
PDI	Polydispersity Index
PDT	Photodynamic Therapy
PI3K	Phosphoinositide 3-kinase

PLA	Poly(Lactic Acid)
PLGA	Poly(lactic–co–glycolic acid)
PNP	Polymeric Nanoparticle
PTT	Photothermal Therapy
PVA	Poly(vinyl alcohol)
RT	Radiation Therapy
SERS	Surface-Enhanced Raman Scattering
SPR	Surface Plasmon Resonance
STEM	Scanning Transmission Electron Microscopy
TGA	Thermogravimetric Analysis
Tg	Glass Transition Temperature

1. INTRODUCTION

1.1 Motivation

The disadvantages encountered in the clinical use of traditional anticancer drugs have led to the need to deliver chemotherapeutics to the tumor area in a controlled manner through external stimulus-triggerable mechanisms, which can result in better patient compliance and treatment outcomes [1],[2]. However, the fact that untargeted heating in thermochemotherapy, one of the combined treatments, produces undesirable results shows the necessity of targeting external stimuli as much as targeting the chemotherapeutic drug [3]. At this point, photothermal therapy, which allows the heat to be precisely localized to the targeted area, achieves this effective result thanks to light and photothermal agents [3].

Generation of photo–hyperthermia effects by near-infrared (NIR) photon irradiation may be provided by various photothermal agents such as gold nanoparticles, carbon nanomaterials, and conducting polymeric nanomaterials. Low absorption coefficients of NIR light in hemoglobin, and water provide long tissue penetration depth [4]. The nanomaterials used as photothermal agents successfully transform the absorbed NIR photons into heat and this energy transformation acts on tumors without damaging normal tissue. In addition to all these, the fact that photo-induced heat has an indirect effect by increasing the sensitivity to chemotherapeutic agents by increasing membrane permeability and blood vessel dilation in the tumor area is a strong factor for the application of this combined therapy [1]. Among plasmonic gold materials, which are photothermal agents, gold nanorods stand out in terms of showing longitudinal surface plasmon resonance (LSPR) in the near infrared light regions that penetrate into the tissue and with its ease of LSPR band tunability [5].

Poly lactic-co-glycolic acid (PLGA), which has FDA-approved formulations, is biocompatible and biodegradable, and provides the flexibility to control drug release kinetics with its varying lactide/glycolide ratio when used as a drug delivery vehicle [6],[7]. Additionally, glass transition temperature (Tg) also has an impact on drug release behavior. With the increasing movement of polymer chains during transition, drug molecules will leak out of the polymer chain cage, which increases the drug release rate [7]. Without any specific external influence, drug-loaded PLGA particles are generally released from the PLGA matrix by passive diffusion, hydrolysis or enzymatic digestion, which can result from several days to months [8]. Considering the heat emitted by photothermal agents during photothermal treatment, the use of PLGA material, which has relatively low Tg value that needs to be reached for passing transition state from glassy to rubbery, is also promising in terms of controllable drug diffusion with active release.

The general aim of this research is to design a light-driven polymeric nanocarrier system loaded with gold nanorods and doxorubicin for use in drug delivery applications and to evaluate the photothermal and cytotoxic effectiveness of the designed system on cancer cells (Figure1.1).

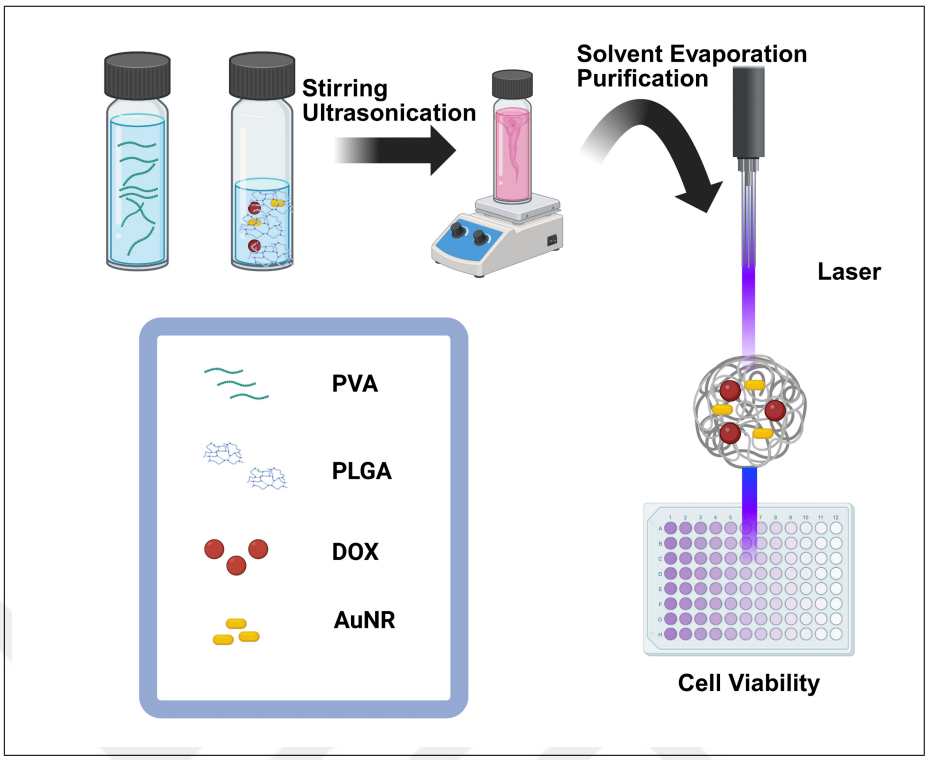

Figure 1.1 General representation of the research.

1.2 Objectives

The primary objective of this thesis is to develop and evaluate a multifunctional polymeric nanoparticle system based on poly(lactic-co-glycolic acid) (PLGA), designed for the co-delivery of gold nanorods (AuNRs) and doxorubicin (DOX), with potential application in combined photothermal and chemotherapeutic cancer treatment. The system aims to achieve high colloidal stability, efficient light-to-heat conversion, and controlled drug release, while maintaining biocompatibility under physiologically relevant conditions.

To achieve this ultimate goal, the following specific objectives were pursued:

Objective-1: Gold nanorods (AuNRs) were synthesized and characterized to ensure suitable size, morphology, and longitudinal surface plasmon resonance (LSPR)

properties for photothermal conversion at 808 nm.

Objective-2: A series of PLGA nanoparticle formulations were prepared by varying the AuNR:PLGA ratio to determine the optimal AuNR loading condition that allows for stable encapsulation without aggregation.

Objective-3: The optimal AuNR-loaded PLGA formulation was identified through comprehensive physicochemical characterization, including scanning transmission electron microscopy (STEM) imaging, dynamic light scattering (DLS), Fourier–Transform infrared spectroscopy (FTIR), and TGA, focusing on homogeneity, morphology, and encapsulation efficiency.

Objective-4: Doxorubicin (DOX) was co-encapsulated into the optimized PLGA-Au nanoparticles, and the dual-loaded system (PLGA-Au-DOX) was evaluated for particle size, polydispersity index (PDI), colloidal stability, and drug loading efficiency.

Objective-5: Long-term stability studies were conducted under different conditions:
(a) colloidal and optical stability of AuNRs after mechanical stress (centrifugation protocols) over 110 days and
(b) pH-dependent buffer storage (pH 7.4, 6.5, 5.5) at 4°C over 300 days.

Objective-6: Photothermal performance of AuNR-loaded nanoparticles was assessed using NIR laser irradiation at different power densities. The thermal response was recorded to evaluate light-to-heat conversion efficiency.

Objective-7: Biocompatibility of PLGA and PLGA-Au nanoparticles was tested using the MTT assay on L929 fibroblast cells, following ISO 10993-5:2020 guidelines.

Objective-8: The combined therapeutic potential (chemotherapy + photothermal therapy) of PLGA-DOX and PLGA-Au-DOX formulations was evaluated in vitro on MCF-7 breast cancer cells, including control comparisons under near–infrared (NIR)

laser exposure.

1.3 Thesis Outline

Five fundamental chapters comprise this thesis. The primary objectives are defined, the motivation for the study is introduced, and the thesis's general structure is outlined in Chapter 1. The principles of photothermal therapy (PTT), the integration of PTT with chemotherapy, drug delivery systems, and the use of PLGA as a biodegradable nanocarrier are all covered in Chapter 2, which also provides a comprehensive context on cancer and the limitations of conventional therapies. These topics serve as the thesis's scientific foundation. The materials and experimental procedures employed in the investigation are detailed in Chapter 3. The synthesis of PLGA nanoparticles, optimization of AuNR loading, co-encapsulation of doxorubicin and AuNRs, physicochemical characterization, drug release experiments, nanoparticle stability analysis, photothermal irradiation studies, and *in vitro* cell culture assays are all included in this chapter. The experimental results are presented and discussed in detail in Chapter 4. The physicochemical stability, drug release profiles, photothermal efficiency, and cytotoxic responses of MCF-7 breast cancer cells are used to assess the performance of the dual-functional nanoplatform. The main findings are summarized in Chapter 5 and a perspective on future research directions is provided. It also underscores the potential of the devised system for additional in vivo applications in dual-modality cancer therapy.

2. RESEARCH BACKGROUND

2.1 Cancer and the Need for Advanced Therapeutic Strategies

Breast cancer (BC) is currently among the most common types of cancer worldwide, and its incidence is anticipated to rise by nearly 50% by 2030, largely due to lifestyle changes and advances in screening technologies. In addition to being a leading cause of death and morbidity among women, the burden of the disease is even greater in developing countries where access to early diagnosis and effective treatment is often limited. Treatment challenges, genetic factors and the rapid progression of the disease are also important factors that contribute to lower survival rates [9],[10].

Breast cancer is characterized using histological classification and molecular classification [11]. The therapeutic strategy for breast cancer is primarily determined by four specific molecular subtypes, defined according to the expression of hormone receptors that affect the prognosis of the disease. The subtypes comprise luminal A, luminal B, triple-negative, and HER2-enriched breast tumors [12]. During the past century, the treatment of people with breast cancer has changed significantly from a purely surgical strategy to a multidisciplinary one that now includes immunotherapy, targeted therapy, endocrine therapy, chemotherapy, and radiotherapy. This change has resulted from a growing comprehension of the illness and the identification of notable, unusual characteristics that set it apart from other forms of cancer [13].

The typical BC treatment regimen includes surgery, chemotherapy, radiation therapy, and endocrine and hormone therapy; however, these methods might have significant side effects and limitations (Figure 2.1) [14]. Regarding the effects on the surrounding problems, breast surgery damages the lymphatic, neurological, and blood vessels, resulting in fibrosis and abnormalities of gait, particularly following unilateral

mastectomy, as well as upper limb lymphedema [15]. Adjuvant therapy, including radiation therapy (RT), is usually used to eliminate any leftover cancer cells and reduce the chance of recurrence after neoadjuvant therapy shrinks the tumor. Even though radiation therapy stops cancer from coming back, because it uses high doses of radiation, it can have negative side effects include decreased feeling, skin irritation, and skin peeling in the treated areas [14].

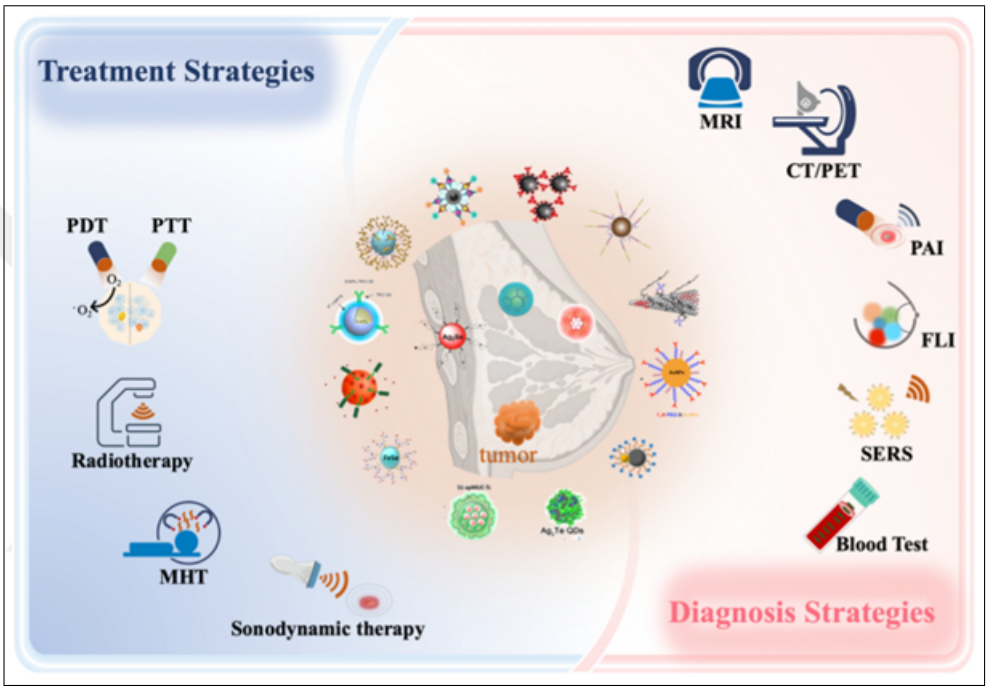

Figure 2.1 A summary of nanotechnology-based strategies for cancer diagnosis and treatment. The left side shows therapeutic approaches like PTT, photodynamic therapy (PDT), and radiotherapy, while the right side highlights diagnostic tools such as Magnetic Resonance Imaging (MRI) and blood tests. The central nanoparticles represent multifunctional systems that can support both diagnosis and treatment[16].

2.2 Limitations of Conventional Chemotherapy

Conventional chemotherapy, long regarded as a cornerstone in the treatment of breast cancer, faces several significant limitations that compromise its overall efficacy and negatively affect patient outcomes as low selectivity, high toxicity, insufficient access of drugs to the target tumor, poor drug solubility and low bioavailability (Figure 2.2). In particular, inadequate drug delivery to the target tumor is one of the main problems that seriously hinders the positive results of chemotherapy [17].

Breast cancer stem cells (BCSCs) develop resistance to both chemotherapy and radiotherapy through drug efflux, DNA repair, anti-apoptotic and antioxidant mechanisms; activation of pathways such as Hippo and PI3K/AKT/NRF2 also supports this resistance [18]. A significant difficulty in cancer therapy is drug resistance, when cancer stem cells demonstrate resilience to chemotherapeutic drugs and stay impervious to treatment, ultimately resulting in tumor recurrence [12].

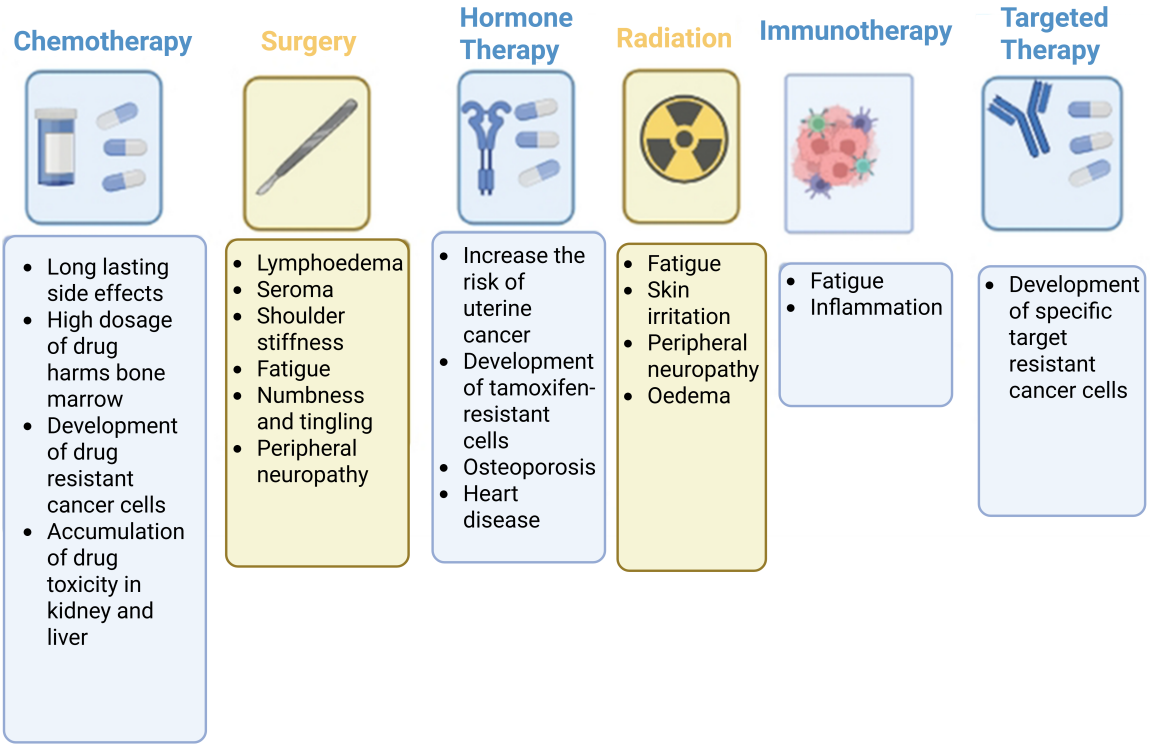

Figure 2.2 Common side effects associated with different cancer treatment modalities. Chemotherapy, surgery, hormone therapy, radiation, immunotherapy, and targeted therapy each come with specific risks, ranging from fatigue and inflammation to drug resistance, organ toxicity, or nerve damage [19].

2.3 Combined Therapy Approaches in Cancer Treatment

The complex nature of cancer requires the implementation of several complementary treatment strategies. Consequently, several combination techniques such as chemo-gene therapy, chemo-radiotherapy, chemo-immunotherapy, chemo-photothermal therapy, as well as combined therapy regimens have been formulated to improve ther-

apeutic efficacy against cancer (Figure 2.3)[20].

Synergistic effects are attempted by carrying more than one therapeutic agent in the same nanocarrier. Co-delivery systems provide better synergy, increase patient compliance, and allow more precise control of the dose of each drug. Thanks to the integration of nanotechnology into this field:

- Biological distribution of drugs is improved,
- The duration of drug residence in the bloodstream is extended,
- Controlled release is provided,
- Drug entry into the cell via endocytosis is allowed to overcome multidrug resistance (MDR).

For this purpose various nanocarriers systems like micellars, liposomes, biodegredable polymer nanoparticles, nanohydrogels and dendrimers are being intensively researched [21].

Nanoparticles incorporating photothermal agents, photosensitizers, or anticancer drugs have been developed to enhance the therapeutic efficacy of chemotherapy combined with PDT or PTT. Following phototherapy, tumor cells can be rapidly destroyed through vascular damage, necrosis, or apoptosis. Nevertheless, because phototherapy alone may not completely eradicate all tumor cells, there is a risk of tumor recurrence. Integrating chemotherapy at this stage can help suppress further tumor progression [22].

The results obtained from studies in the literature using gold nanorods as photothermal agents and combined with chemotherapeutic drugs are promising [23],[1],[24].

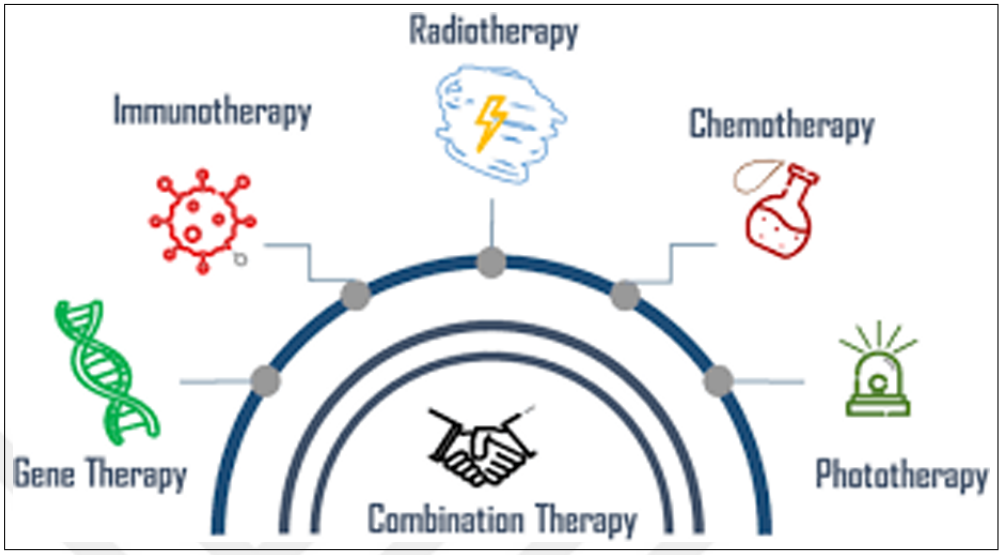

Figure 2.3 Illustration of various cancer treatment strategies, including immunotherapy, radiotherapy, chemotherapy, gene therapy, and phototherapy. At the center, combination therapy is highlighted as an integrative approach that brings together multiple treatment methods to improve therapeutic outcomes [25].

2.4 Principles of Photothermal Therapy (PTT)

The facile, controllable, and noninvasive characteristics of photothermal therapy (PTT), which is based on photothermal compounds to absorb near-infrared light and generate heat, have garnered significant research interest in cancer treatment [26]. Since tumor cells are more heat-sensitive compared to healthy cells, they can be selectively eliminated through this technique. Typically, laser systems are employed in PTT to induce controlled thermal damage in the affected tissue [12].

Few research have examined the basic biological responses to PTT, such as whether dying cells undergo the apoptotic or necrotic route whereas, most have focused on operational therapeutic effects. Necrosis and apoptosis are well-known yet distinct cell death mechanisms. Necrosis destroys cellular activities and cell membrane integrity, allowing potentially cytotoxic or antigenic contents to escape into the extra-

cellular space. Leakage can cause inflammatory responses that damage surrounding tissues or cause tumor growth. In contrast, the cell cycle includes apoptosis. Apoptotic cells have intact plasma membranes, therefore cytoplasmic contents rarely leak, preventing cell and tissue harm. Apoptotic cells also release some indicators on their cell membranes, which phagocytes use to preferentially recognize and quickly engulf them. For these reasons, apoptosis is seen as the "cleaner" cell death method [27]. As the ambient temperature rises to 42°C, protein denaturation and transient cellular inactivation occur (Figure 2.4). Between 43 and 45°C, prolonged cellular inactivation and localized oxidative stress are observed, leading to the initiation of apoptosis in cancer cells. When the temperature reaches around 46°C, rapid necrosis begins, a process referred to as thermoablation. Further heating to 48–60°C causes immediate cellular death due to microvascular thrombosis and ischemia [20],[28]. While the intricate mechanisms of thermoablation remain incompletely elucidated, it is well acknowledged that temperature-induced denaturation of the cell membrane and cytoplasmic proteins is pivotal in cellular death [20].

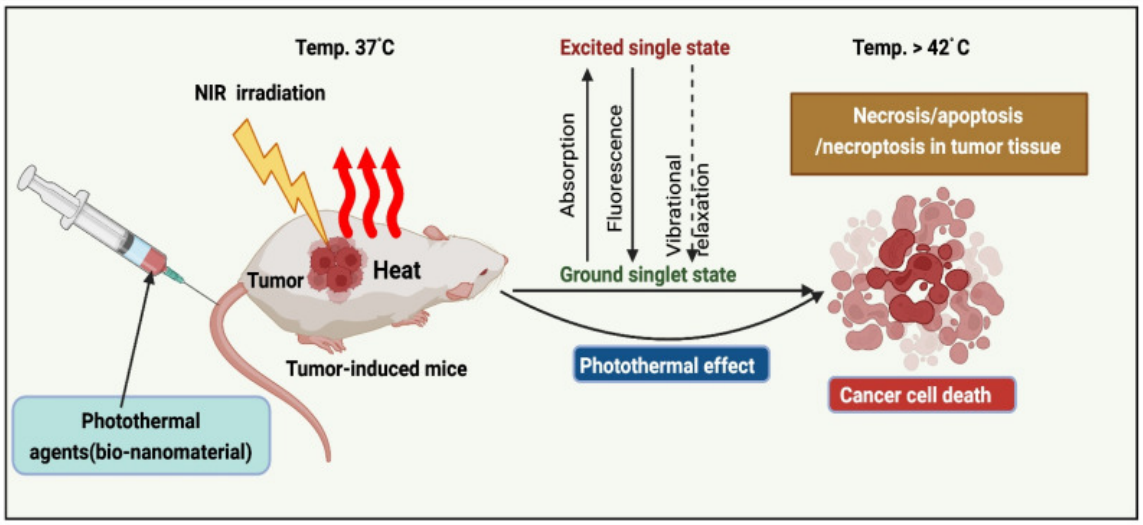

Figure 2.4 Schematic representation of the photothermal therapy mechanism. Photothermal agents are injected into tumor-bearing mice and activated by near-infrared (NIR) irradiation. The resulting heat raises the tumor temperature above 42°C, leading to cancer cell death through necrosis, apoptosis, or necroptosis [29].

In recent years, near-infrared (NIR) light-responsive materials have garnered significant attention in the field of cancer photothermal therapy. Because NIR light within the 650–900 nm wavelength range is weakly absorbed by skin and tissues, it

enables deeper tissue penetration without causing damage. Additionally, NIR-based photothermal therapy offers a non-invasive treatment option that preserves surrounding healthy cells. Several notable photothermal agents have been specifically designed for this purpose. Materials such as gold nanocages, carbon nanotubes, gold nanoshells, and gold nanorods efficiently absorb NIR light and convert it into thermal energy, inducing cytotoxic effects on cancer cells. Among these agents, gold nanorods are particularly promising due to their tunable longitudinal absorption in the NIR region and their easily modifiable surface properties [30]. GNRs have two surface plasmon peaks, with the weaker, untunable peak corresponding to the visible light transverse SPR frequency due to their shape. The GNR aspect ratio (length:width) tunes the second peak in the near-infrared region (NIR), which corresponds to the stronger longitudinal surface plasmon resonance (SPR) frequency. At peak SPR frequency, GNRs absorb and scatter strongly, which can be used for imaging and therapy. The tissue optical window (600–1000 nm) produces less endogenous scattering and absorption interference, making it ideal for biological applications [31]. However, to ensure effective tumor accumulation through the enhanced permeability and retention (EPR) effect and to achieve efficient tumor ablation, challenges such as heterogeneous heat distribution within the tumor and the necessity for high laser power must also be carefully considered [30]. Also, the biocompatibility and certain deficiencies in photothermal characteristics restrict its utilization. The presence of a toxic cetyltrimethylammonium bromide (CTAB) molecular layer on the surface makes it unfavorable for direct photothermal therapy. Furthermore, its structure will collapse and change under laser irradiation and the advantageous NIR window of the GNRs may transition to the visible spectrum due to the commonly seen aggregation and clustering of the GNRs inside various cells leading to a reduction in photothermal efficacy [32],[33]. Consequently, enhancing biocompatibility and photothermal stability creates a significant barrier for the photothermal application of gold nanorods [32]. Therefore, various nanoscale encapsulation systems have been engineered to encapsulate coat gold nanorods (GNRs) and demonstrate their distinctive and amplified therapeutic effects through thermal ablation of tumors (Figure 2.5) [33],[34].

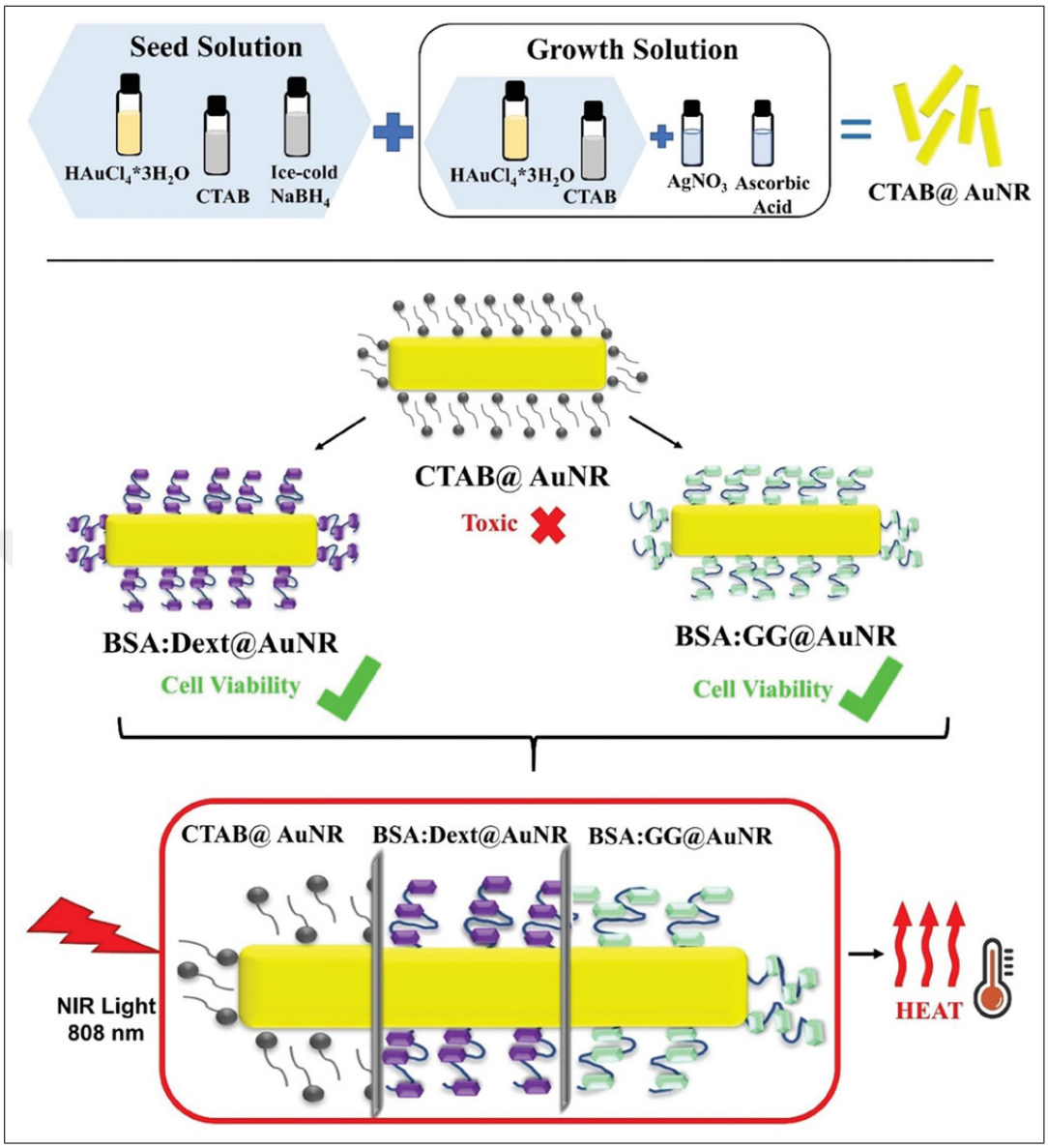

Figure 2.5 Synthesis and surface modification of gold nanorods (AuNRs) for photothermal therapy. AuNRs synthesized using CTAB show cytotoxicity, while coating with BSA:Dextran or BSA:Gum Arabic (GG) improves biocompatibility. Upon 808 nm NIR irradiation, all AuNR formulations generate heat, demonstrating their photothermal potential [34].

2.5 Photo-Chemotherapy: Integration of PTT and Chemotherapy

Traditional cancer treatment methods such as chemotherapy and radiotherapy, which cause serious side effects due to high doses and intense radiation, reduce the

patient's quality of life and cause a decrease in treatment success. Therefore, the increasing need for more effective and less side-effect treatments has paved the way for the development of non-invasive approaches such as magnetic hyperthermia, photothermal therapy and photodynamic therapy. In particular, the combination of photothermal therapy and chemotherapy is on the agenda as a remarkable application [35]. The integration of chemotherapy with photothermal therapy, one of the combined treatments, stands out with its ability to reduce the development of drug resistance and to reduce systemic side effects. Photosensitive nanostructures increase the sensitivity of cells that are already responsive to chemotherapy by producing localized heat. Small drug molecules can be chemically bound to structures that react to light using different synthetic methods or encapsulated inside them. After NIR application, the drugs together with the nanostructure are released in a controlled manner and provide targeted drug accumulation in the tissue (Figure 2.6)[20].

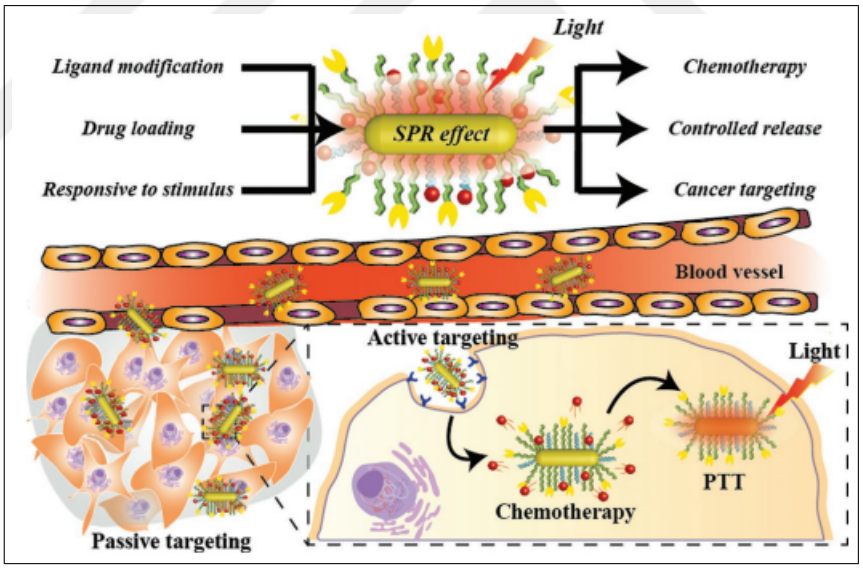

Figure 2.6 Schematic illustration of the synergistic action of CHT and PTT utilizing GNRs [30].

Gold nanorods hold promise for both drug delivery systems and direct photothermal cancer therapy due to their strong optical and photothermal properties; they also have potential for advanced sensing technologies such as surface-enhanced Raman scattering (SERS) [36]. Particle size, shape, and the metal's dielectric constant all affect the surface plasmon resonance (SPR) of gold nanoparticles, which is caused by a collective coherent resonant oscillation in the presence of the oscillating

electromagnetic field of the light (Figure 2.7) [37]. A recent study investigated in gold nanorods were encapsulated within PLGA and further functionalized with folic acid to enhance biocompatibility and tumor targeting efficiency. The resultant nanostructures maintained significant NIR absorbance and effective photothermal conversion, while demonstrating enhanced cell survival, thereby affirming their appropriateness for therapeutic applications [38].

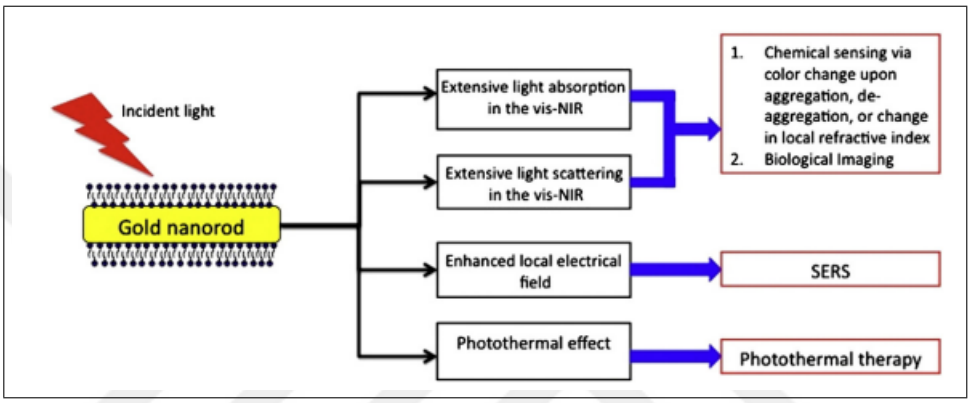

Figure 2.7 Schematic illustration of the light-induced optical properties of gold nanorods and their applications. Upon light exposure, gold nanorods exhibit strong absorption and scattering in the visible to NIR range, enhanced local electric fields, and photothermal effects. These properties enable applications such as chemical sensing, biological imaging, surface-enhanced Raman scattering (SERS), and photothermal therapy [36].

Doxorubicin (DOX) is an important chemotherapy drug developed in the 1960s and approved by the FDA in 1974. DOX, which belongs to the anthracycline group, is naturally red-orange in color and water-soluble. It is used in the treatment of many types of cancer, including breast cancer, ovarian cancer, soft tissue and bone sarcomas, leukemia and lymphoma in adult and pediatric patients. Its basic mechanism of action is to stop cell proliferation by inhibiting the topoisomerase II enzyme, which is responsible for DNA replication in cancer cells. DOX, which has strong anticancer properties, is subject to dose limitation or treatment interruption due to its serious side effects. Various nanoformulation strategies such as liposomes, dendrimers, solid lipids and lipid nanoparticles have been developed as a solution to this situation (Figure 2.8). In this way, it is aimed to improve both drug delivery and reduce systemic toxicity [36],[39]. Tsai et al. engineered a doxorubicin-loaded PLGA nanoparticle with a surface in addition decorated with cationic and anionic polyelectrolytes, significantly

enhancing colloidal stability and *in vitro* anticancer efficacy [40].

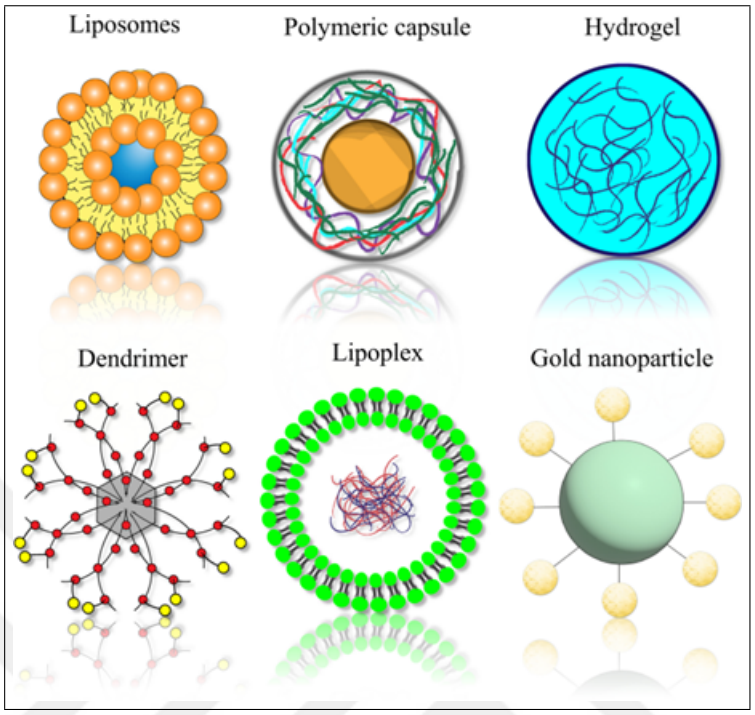

Figure 2.8 Representation of nanoformulation that can be loaded with DOX [41].

2.6 Drug Delivery Systems for Cancer Therapy

In recent years, there has been growing interest in drug delivery systems that utilize nanomaterials capable of responding to environmental stimuli and offering controlled drug release within the body. "On-demand" drug delivery platforms, designed to meet individual patient needs, allow for precise spatial and temporal regulation of therapeutic release at specific sites over defined periods. However, conventional drug delivery systems still encounter major obstacles, such as limited control over release profiles, challenges in drug-organ compatibility, and difficulties in production processes, often leading to inefficient and non-specific drug distribution. Additionally, differences in chemical environments across various organs make oral delivery unsuitable for many drugs, while adverse effects on non-target tissues remain a critical issue. To overcome these limitations, implantable delivery systems have been developed, providing direct access to tumors and enabling localized therapeutic interventions. Moreover, stimulus-responsive nanomaterials significantly enhance the effectiveness of cancer treatments

by supporting the creation of more sophisticated and targeted delivery strategies (Figure 2.9) [42].

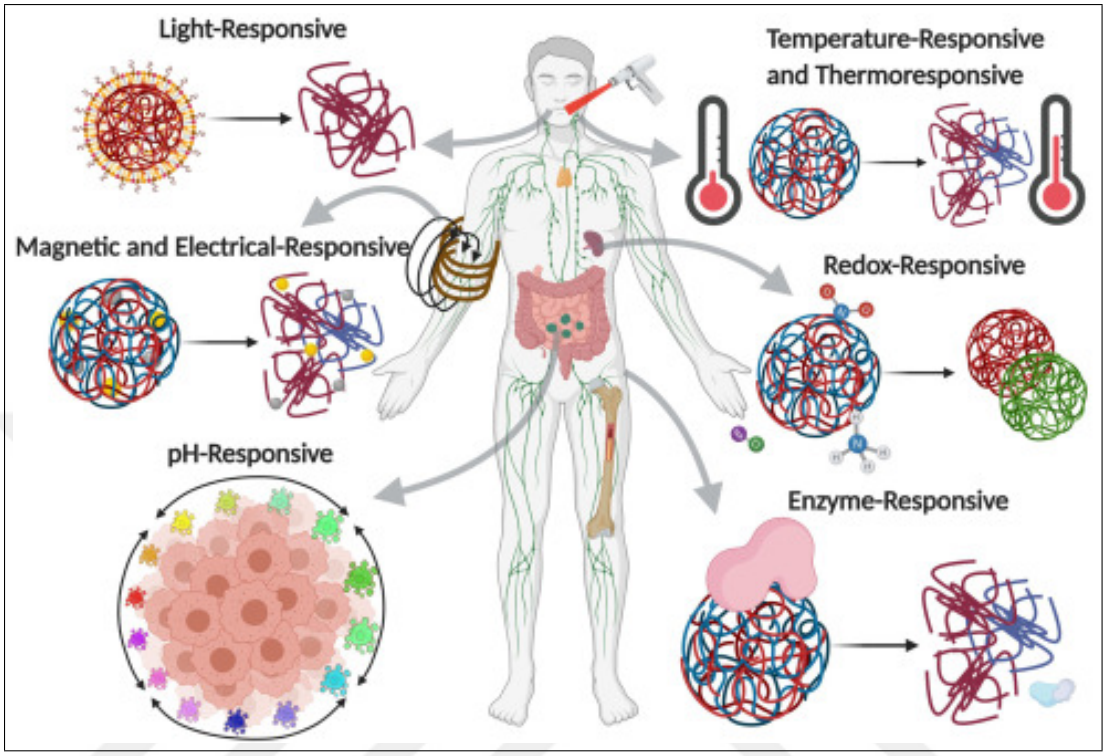

Figure 2.9 Schematic illustration of stimuli-responsive drug delivery systems. Nanocarriers can be engineered to release therapeutic agents in response to specific triggers, including light, temperature, magnetic or electrical fields, redox conditions, enzymatic activity, and pH changes. These smart systems enable controlled, site-specific, and efficient drug release, enhancing therapeutic outcomes while minimizing off-target effects [43].

Many different kinds of pharmaceuticals can be administered using nanoparticles, including hydrophilic and hydrophobic small compounds, vaccinations, and biological macromolecules [44]. The controllability of parameters such as size, surface properties, and biocompatibility allows these systems to precisely regulate drug release of polymeric nanoparticles (PNPs). PNPs hold promise in the treatment of diseases such as cancer due to their potential to overcome biological barriers and provide stimuli-responsive drug release. However, manufacturing difficulties and barriers to integration into clinical applications limit the wider use of this technology[45].

A wide range of synthetic and natural biodegradable polymers exists. Starch, albumin, gelatin, sodium alginate, and chitosan are examples of natural biodegrad-

able polymers [46]. Other commonly used polymers include poly(lactic acid) (PLA), poly(lactic-co-glycolic acid) (PLGA), poly(-caprolactone) (PCL) and polyanhydrides, each of which offers different degradation rates and drug delivery properties. Methods such as nanoprecipitation, emulsion-evaporation and spray drying from solution are used in the preparation of PNPs, and these production techniques have a direct effect on the morphology, drug loading capacity and release kinetics of the carrier. Especially in cancer treatment, PNPs are used to increase therapeutic efficacy by reducing systemic toxicity [47]. To our knowledge, the study by Chuang et al. is the sole report evaluating a PLGA/DOX/AuNR system as a drug delivery vehicle in MCF-7 cells [1]. Unlike the HADP nanocomplexes that required additional HSA coating, our PLGA-AuNR-DOX formulation achieves stable encapsulation through a more straightforward design, underscoring its novelty and practical advantage. Also, in that study, the optimization of gold-nanorod loading and the evaluations of long-term nanoparticle stability were not conducted. This disparity is prevalent not only in that work but also in other research that integrates a polymer matrix, gold nanorods, and a chemotherapeutic drug [23],[1],[24]. These studies demonstrate the effectiveness of drug delivery systems in cancer treatment.

2.7 PLGA as a Biodegradable Carrier

Poly(lactic-co-glycolic acid) (PLGA) is a synthetic copolymer synthesized from lactic acid and glycolic acid monomers, widely recognized for its significant success in drug delivery and tissue engineering applications [39]. PLGA is highly biocompatible and biodegradable in the human body; its breakdown products, CO2 and H2O, are non-toxic and removed from the body by the Krebs cycle. The degradation of ester linkages through hydrolysis in aqueous environments is regulated by polymer chemistry factors, including glycoside unit concentration, initial molecular weight (MW), stereochemistry (d and l composition), and end-group functionalization (Figure 2.10) [48]. Among its notable advantages are its complete biodegradability in aqueous environments, regulatory approvals from both the FDA and EMA for parenteral drug delivery, protection of drugs from degradation, and its ability to enable sustained and targeted

release. Nevertheless, despite achieving high encapsulation efficiency, the commercialization of PLGA nanoparticles remains limited, primarily due to their low drug loading capacities. This challenge is even more critical when working with hydrophilic drugs such as doxorubicin [39].

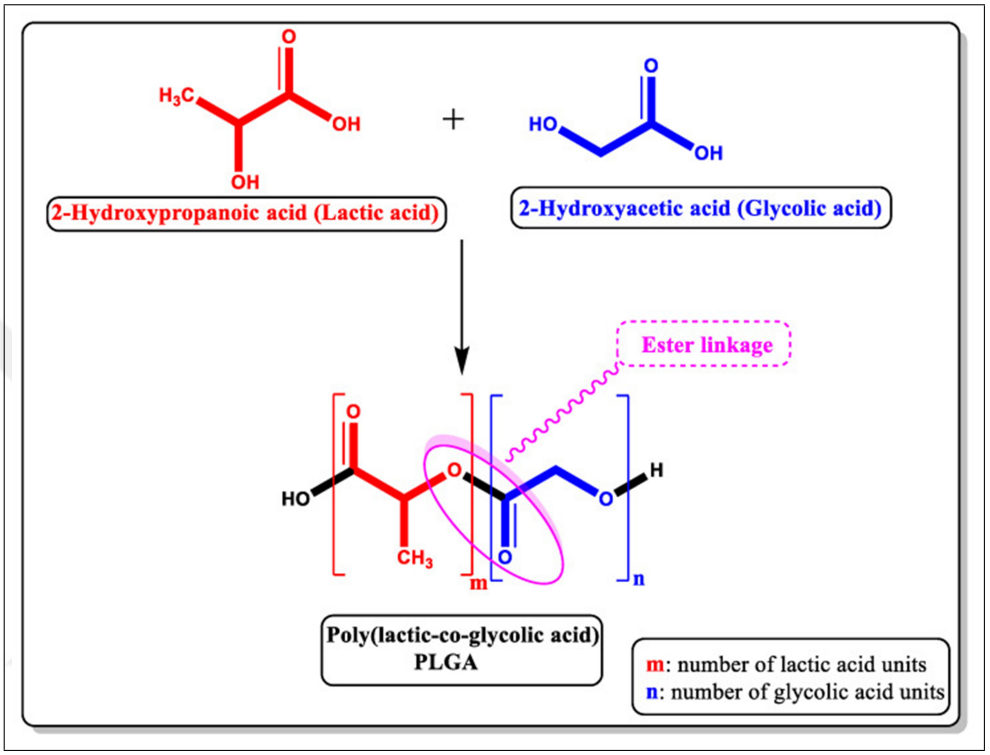

Figure 2.10 Chemical structural diagram for PLGA and its monomers. Owing to the existence of ester bonds that undergo hydrolysis in watery settings [48].

In an aqueous environment, PLGA is subjected to hydrolytic degradation, which results in the random hydrolysis of ester linkages that are present along the polymer backbone. One carboxylic acid group and one hydroxyl group are generated by each hydrolyzed ester linkage. The molecular weight of the polymer is reduced as a result of the scission of long polymer chains, which increases its hydrophilicity. Subsequently, the polymer forms water-soluble fragments. These water-soluble fragments are hydrolyzed to lactic and glycolic acids, which are subsequently decomposed to produce energy, carbon dioxide, and water through the body's typical metabolic pathways. The degradation mechanism of PLGA is significantly influenced by the monomer ratio of lactic:glycolic acid. For example, the hydrophobic lactide content of PLGA 85:15 is higher than that of PLGA 50:50, which results in a more rapid rate of degrada-

tion [49]. The PLGA end group also contributes to polymer breakdown. The acidic terminal group of PLGA facilitates the hydrolysis of ester bonds, resulting in the formation of more acidic groups in an autocatalytic cycle throughout the degradation process. Consequently, the PLGA containing an acidic terminal group degrades far more rapidly than its ester-ended counterpart [50]. The glass transition temperature (Tg) of PLGA is similarly associated with its lactic acid to glycolic acid (LA:GA) ratios. The glass transition temperature (Tg) of polymers denotes the temperature at which they transition from a glassy state (below Tg) to a rubbery one (above Tg). Given that the Tg of PLGA is approximately 50 °C, which exceeds physiological temperature, it is typically defined by the mechanical strength and rigidity of its composition. The glass transition temperature (Tg) rises with higher polymer molecular weights and increased lactic acid (LA) content [51].

Table 2.1
Key physicochemical and degradation-related properties of PLGA.

Property	**Description**
Composition (LA:GA ratio)	The most common ratio is 50:50. Higher GA content increases hydrophilicity and accelerates degradation.
Melting Temperature	The melting point decreases with increasing GA fraction, enabling the fabrication of diverse structures.
Solubility	PLGA is soluble in various organic solvents (e.g., dichloromethane, acetone); solubility decreases as GA content increases.
Glass Transition Temperature (Tg)	Approximately 50°C. Tg increases with higher molecular weight and LA content, enhancing mechanical rigidity.
Crystallinity	PLGA is primarily amorphous, facilitating homogeneous drug distribution and controlled release.
Molecular Weight and Viscosity	Higher molecular weight correlates with increased viscosity. Molecular weights between 15–100 kDa correspond to degradation over weeks to months.
Degradation Mechanism	Mass loss occurs through hydrolysis of ester bonds, water absorption, and polymer chain scission.
Autocatalytic Effect	Carboxyl end groups generated during degradation catalyze further hydrolysis; PLGA–COOH degrades faster than end-capped PLGA.
Biological Influences	Adsorption of proteins, cell accumulation, and free radical production can accelerate *in vivo* degradation.
Biodegradation Products	Lactate and glycolate are eliminated via the Krebs cycle or excreted in urine.
pH Influence	Degradation and drug release are enhanced under alkaline conditions (high pH) [51].

3. EXPERIMENTAL SECTION

3.1 Materials

Poly(lactic-co-glycolic acid) (PLGA, Resomer RG 503H; lactide:glycolide 50:50, acid-terminated, molecular weight 24–38 kDa) was acquired from Sigma-Aldrich. Chloroform (ACS reagent, ≥99.8%) was obtained from Fisher Scientific. Poly(vinyl alcohol) (PVA; M_w 13–23 kDa, 87–89% hydrolyzed) was provided by Sigma-Aldrich. Doxorubicin hydrochloride (DOX·HCl) was acquired from Biosynth Carbosynth. Dulbecco's phosphate-buffered saline (DPBS) was procured from Gibco, a division of Thermo Fisher Scientific. A dialysis membrane with a molecular weight cutoff of 6000–8000 was acquired from Carl Roth.

For cell culture investigations, Dulbecco's Modified Eagle's Medium (DMEM), fetal bovine serum (FBS, sourced from Brazil), Penicillin-Streptomycin (10,000 U/mL, 100×), and Trypsin-EDTA (0.25% with phenol red) were procured from Gibco; Dimethyl sulfoxide (DMSO, cell culture reagent) was obtained from NutriCulture; Thiazolyl Blue Tetrazolium Bromide (MTT Reagent, 98%) was acquired from Thermo Fisher; and Trypan Blue was sourced from Hyclone.

3.2 Synthesis of PLGA Nanoparticles

PLGA nanoparticles were synthesized utilizing a miniemulsion process adapted from a previously reported protocol in our laboratory [52]. To create the organic (dispersed) phase, 50 mg of PLGA was dissolved in 2.5 mL of chloroform. Simultaneously, the aqueous phase was prepared by dissolving 75 mg of poly(vinyl alcohol) (PVA) in 10 mL of Milli-Q water with continuous agitation. The aqueous phase was gradually added to the organic phase while being magnetically agitated at 1000 rpm at room temperature (25 °C) for 1 hour to form a macroemulsion. Ultrasonication was subse-

quently performed in an ice bath for 2 minutes using a Branson Sonifier (450 W) at 70% amplitude, with 10-second on/off cycles to generate a stable miniemulsion. The organic solvent was subsequently evaporated by agitating the emulsion at 300 rpm for 16 hours at room temperature, leading to the formation of PLGA nanoparticles.
Gold nanorods (AuNRs) were manufactured by a seed-mediated growth method as described by Zengin et al. [34]. Gold nano seeds were synthesized by reducing 0.01 M $HAuCl_4{\cdot}3H_2O$ solution with 0.01 M ice-cold $NaBH_4$ in the presence of 0.1 M cetyltrimethylammonium bromide (CTAB). The mixture was gently stirred and subsequently incubated at 30°C in a water bath. To prepare the growth solution, 0.01 M $HAuCl_4$ was combined with 0.1 M CTAB, 0.1 M $AgNO_3$ and 0.1 M L(+)-Ascorbic acid, respectively. Finally, the seed solution was incorporated into the growth solution. The resulting solution was maintained for 3 hours in a 30°C water bath. After 3 hours, the solution was subjected to centrifugation at 4000 rpm and preserved at +4°C. The technique carried out without modification, and all compounds (same lot number) and concentrations utilized were in accordance with those outlined in the original protocol.

3.3 Optimization of Gold Nanorod Encapsulation

To ascertain the optimal gold loading ratio for dual therapy applications, gold nanorods (AuNRs) were encapsulated at varied mass ratios of 5%, 10%, 14%, 27%, and 41% relative to a fixed PLGA mass. The quantity of AuNR corresponding to the specified weight was determined using the established calibration curve (Figure A.1.A), and the calculated volume of gold nanorods was subjected to centrifugation at 12,000 rpm for 15 minutes. PLGA was dissolved in chloroform, and the centrifuged AuNRs were incorporated into the vial and mixed at 1600 rpm for one minute to achieve the dispersed phase. The aqueous phase, containing PVA dissolved in Milli-Q water, was incrementally introduced into the dispersed phase while stirring at 1000 rpm. The macroemulsion was subsequently created by continuous agitation at 1000 rpm for one hour at 25 °C. Afterwards, AuNR-encapsulated PLGA nanoparticles were subjected to centrifugation twice for 30 minutes at 6000 rpm, after which the pellet was re-dispersed in Milli-Q water.

3.4 Combined Encapsulation of Gold Nanorods and Doxorubicin

By the miniemulsion technique, a final concentration of 1 mg/mL of doxorubicin-hydrochloride (DOX) and 0.714 mg/mL of gold nanorod-encapsulated PLGA nanoparticles was produced. The amount of AuNR corresponding to 7.14 mg was determined as described in Section 3.3. DOX (10 mg) was first dissolved in 0.3 mL of DMSO, then PLGA (50 mg) dissolved in 2.5 mL of chloroform and centrifuged AuNRs were added and mixed at 1600 rpm for one minute to obtain the dispersed phase. The next steps of the synthesis were conducted as per the methodology described in Section 3.3. The encapsulated Dox content was spectrophotometrically evaluated at 480 nm using the Infinite M1000 microplate reader (Tecan, USA) based on the absorbance of the supernatants. DPBS was used to dilute the supernatants in a 2:5 (sample:total) (v:v) ratio. The previously established Dox calibration curve was utilized to determine the concentration corresponding to the absorbance value (Figure A.1.B).

The amount of encapsulated gold nanorods (AuNRs) in the nanoparticle formulations was quantified by thermogravimetric analysis (TGA). Measurements were conducted in a nitrogen atmosphere utilizing a TGA55 apparatus (TA Instruments). In platinum pans, 1.036 mg of lyophilized PLGA-Au-DOX nanoparticles were subjected to heating up to 800 °C at a rate of 10 °C/min. The residual mass at 600 °C was employed to determine the gold concentration in the AuNR-loaded formulations.

A CTAB-stabilized gold nanorod solution was created for lyophilization at a final concentration of 0.714 mg/mL, as indicated by the calibration curve (Figure A.1.A). A specified volume of this solution was lyophilized, resulting in a dried mass of 0.172 mg, which was subsequently evaluated under identical TGA conditions to ascertain the residual gold content.

3.5 Characterization of Nanoparticles

The hydrodynamic diameter of the nanoparticles was determined using a dynamic light scattering (DLS, Zetasizer Lab, Malvern Instruments, U.K.) at a fixed scattering angle of 90°. The values were presented as intensity-weighted average size (Z-average). To ensure optimal count rates and minimize multiple scattering effects, 50 µL of nanoparticle suspension was diluted with 950 µL of Milli-Q water (1:20, v/v) for each measurement. Zeta potential (ζ-potential) measurements were conducted utilizing the same device in a 1 mM KCl solution (1:21, v/v) to maintain a consistent ionic environment. To prevent damage to the zeta cuvette, the number of measurement runs was limited to a maximum of 40.

Morphological characterization of the nanoparticles was performed using scanning transmission electron microscopy (STEM) with a Quatra S instrument (Thermo Fisher Scientific). For STEM analysis, diluted nanoparticle solutions were deposited onto 300-mesh carbon-coated copper grids. The obtained STEM images of AuNRs were analyzed using ImageJ software to measure the length and width of individual nanorods [53].

The optical properties of the synthesized gold nanorods were evaluated using a TECAN Infinite M Nano microplate reader within an absorbance range of 230–1100 nm. FTIR spectroscopy was carried out using the Shimadzu IR Spirit-T spectrometer. The encapsulation efficiency (EE) of AuNR based on TGA analysis was calculated using Eq. 3.1.

$$\%EE = \frac{\text{Amount of encapsulated Au (mg)}}{\text{Amount of Au initially used (mg)}} \tag{3.1}$$

3.6 In Vitro Doxorubicin Release

Using the dialysis method, the *in vitro* release profile of doxorubicin (DOX) was assessed for both PLGA-DOX and PLGA-Au-DOX nanoparticle formulations. After that, the dialysis membranes were filled with the nanoparticle suspension (1 mL) with a molecular weight cut-off (MWCO) of 6–8 kDa. Beakers filled with 13 mL of Dulbecco's Phosphate Buffered Saline (DPBS, pH 7.4) were used to submerge the dialysis bags. The release media was kept at 37 °C and agitated at 300 rpm utilizing a temperature-controlled magnetic stirrer. Samples (600 µL) of the release media were collected at specified intervals: hourly during the initial 4 hours, then approximately every 24 hours until 96 hours. After each sampling, an equivalent volume (600 µL) of fresh DPBS was introduced to preserve sink conditions and maintain a consistent volume.

The DOX content in each sample was determined by measuring absorbance at 480 nm with a UV-Vis spectrophotometer (Infinite M Nano, TECAN, USA), following the equilibration of the samples to room temperature. The concentration of DOX was determined utilizing a previously constructed calibration curve (Figure A.1.B). Notably, no spectral interference was detected during DOX quantification since the gold nanorods (AuNRs) enclosed in the PLGA-Au-DOX formulation do not show a distinctive absorbance peak at 480 nm. Consequently, the UV-Vis signal at 480 nm is solely ascribed to the released DOX.

3.7 Buffer- and RPM-Based Stability Analysis of Nanoparticles

Two distinct stability tests were conducted to assess the behavior of nanoparticles under varying environmental and mechanical conditions. Each study was designated a unique code for clarity and consistent reference throughout the thesis. The STB-Buffer (Stability-Buffer) concentrated on evaluating the stability of PLGA nanoparticles across various buffer systems, including sodium acetate, sodium phosphate, and

phosphate-buffered saline, with differing pH levels. Conversely, STB-Rpm (Stability-Rpm) assessed the influence of several centrifugation methods on the stability of gold nanorods. PLGA nanoparticles and gold nanorods underwent successive centrifugation at different speeds, subsequently followed by storage and observation.

3.7.1 STB-Buffer

To assess the structural stability of the encapsulated systems, synthesized free PLGA nanoparticles were kept at 4 °C in three distinct buffer media (pH 7.4, 6.5, and 5.5 sodium phosphate buffer, and phosphate-buffered saline, respectively) and sampled at predetermined intervals (Figure 4.9.A). After the nanoparticle was synthesized, two consecutive centrifugation cycles were performed on 2.5 mL of nanoparticle suspension at 6000 rpm for 30 minutes. Subsequent to each cycle, the pellet was resuspended in 2.5 mL of fresh buffer and stored at 4 °C. Stability was evaluated by tracking changes in hydrodynamic diameter and polydispersity index (PDI) by dynamic light scattering (DLS) and UV-VIS measurements over time.

3.7.2 STB-Rpm

The STB-Rpm study was formulated based on the cumulative centrifugation stages to which gold nanorods (AuNRs) are subjected during their manufacture and subsequent processing into PLGA-Au nanoparticles. Consequently, two distinct centrifugation methods were developed and evaluated during this study. RPM1 encompasses centrifugation procedures start with an initial spin at 4000 rpm, commonly utilized during AuNR production, followed by 12000 rpm. It denotes the state of unencapsulated AuNRs immediately before the encapsulation. In the RPM2 condition, following the 4000 rpm and 12000 rpm steps, two further centrifugation cycles at 6000 rpm were performed. The RPM2 setting was applied to both free AuNRs and PLGA-Au formulations. RPM2 therefore signifies the ultimate cleaned state of the formulations.

3.8 In Vitro Photothermal Irradiation and Heat Profiling

Using a continuous-wave (CW) diode laser tuned to 808 nm with power densities of 0.5, 0.75, and 1 Wcm^{-2}, 0.3 mL of PLGA Np, gold nanorod (AuNR), PLGA-Au Np, and PLGA-Au-DOX Np suspensions were placed in transparent microcentrifuge tubes and subjected to radiation for 300 seconds. The previously created calibration curve was used to calculate the AuNR content (Figure A.1.A). All experiments were performed in triplicate (n = 3). The thermal camera (FLIR E5 XT Wifi) is positioned at a 90-degree angle relative to the laser and the sample surface. The laser power density was verified using a calibrated power meter (Newport Model 1918-R). The laser point size was established at 0.5 cm^2, ensuring comprehensive coverage of the sample's upper surface. FLIR Tools software was used to determine the peak temperatures during the 30-second intervals of thermal imaging.

3.9 Cell Culture

This study utilized MCF-7 human breast cancer cells (ATCC HTB-22) and L929 murine fibroblast cells (ATCC CCL-1). Both cell lines were cultivated in high-glucose Dulbecco's Modified Eagle Medium (DMEM, Gibco), augmented with 10% (v/v) fetal bovine serum (FBS, Gibco) and 1% penicillin/streptomycin (Gibco). Cells were sustained at 37°C in a humidified incubator with a 5% CO_2 environment (Nüve EC160, Turkey). Cells were detached for passage using 0.25% trypsin-EDTA (Gibco) for 5 minutes under standard incubation conditions. The enzymatic process was inhibited by the introduction of complete growth media, and the cell suspension was centrifuged at 1000 rpm for 5 minutes. The supernatant was discarded, and the cell pellet was reconstituted in fresh media. Cell vitality and density were assessed using an automated cell counter (BIO-RAD TC20) with trypan blue staining.

3.10 Cell Viability (MTT) Assay

Cytotoxicity was evaluated per ISO 10993-5:2020 with L929 murine fibroblast cells (ATCC CCL-1) as the standard cell line. Cell viability was assessed using the 3-(4,5-dimethylthiazol-2-yl)-2,5-diphenyltetrazolium bromide (MTT) test. Ten thousand cells were inoculated into each well of 96-well plates containing 100 μL of full growth medium. After a 24-hour incubation period, the medium was replaced with fresh media containing nanoparticles at varying concentrations (10 to 150 μg mL^{-1}), and the cells were subsequently incubated for a further 24 or 48 hours.

DMSO served as the blank, whereas untreated cells cultivated just with complete media acted as the negative control group. After each incubation period, the media was discarded, and 100 μL of PBS was utilized to gently rinse the cells. Subsequently, 100 μL of fresh DMEM, augmented with 10 μL of MTT solution (5 mg/mL) (MTT reagent, 98%, Thermo Fisher), was added to each well. After a 4-hour incubation, the media was carefully removed, and the resulting formazan crystals were dissolved in 100 μL.

Absorbance was measured at 570 nm using a Bio-Rad iMark microplate reader. Six tests were conducted for each condition, and the findings were expressed as mean $\pm$ standard deviation.

3.11 Photothermal Cytotoxicity in MCF-7 Breast Cancer Cells

Both groups were seeded on the same 96-well plate for each nanoparticle group in order to guarantee that the laser-exposed and non-exposed cells were exposed to the same experimental circumstances, including any possible environmental changes during irradiation. This configuration enabled all wells to experience identical handling procedures, including temporary removal from aseptic conditions during laser expo-

sure. Nanoparticles were introduced at specified doses (150 μg mL^{-1} and 250 μg mL^{-1}) following a 24-hour cell adhesion period. To reduce thermal interference, one blank well was maintained between each sample well. Following 24 hours of nanoparticle incubation, the wells were rinsed with dPBS and replenished with fresh media. Wells allocated for photothermal treatment were irradiated with an 808 nm laser at 1 W cm^{-2} for 300 seconds, whereas the other wells were maintained under identical external conditions without laser exposure. Following a 24-hour incubation period to facilitate drug release from the polymer matrix, the plates were subjected to an MTT-based viability assessment.

Before determining the laser parameters for photothermal treatment, control tests were performed to evaluate the impact of laser exposure alone on cell viability. MCF-7 cells cultured in 96-well plates (without nanoparticle) were subjected to near-infrared (NIR) laser irradiation at differing power densities and durations: 1 W/cm^2 for 5 minutes, 1.7 W/cm^2 for 5 minutes, and 2 W/cm^2 for 5 and 10 minutes. Subsequent to irradiation, the cells were cultured for 24 hours under conventional culture conditions.

3.12 Statistical Analysis

Statistical analyses were performed using OriginPro 2025 (OriginLab Corporation, Northampton, MA, USA). For experiments in which only cells were exposed to laser irradiation ($n = 3$), data were analyzed by one-way ANOVA followed by Tukey's post hoc test, with a significance threshold of $p < 0.01$. For experiments in which nanoparticle-treated cells were subjected to laser irradiation ($n = 3$), a three-way ANOVA followed by Tukey's post hoc test was applied, with $p < 0.05$ considered statistically significant. All results are presented as mean $\pm$ standard deviation (SD).

4. RESULTS AND DISCUSSION

4.1 Fabrication of PLGA Nanoparticles and Parameter Tuning for AuNR Loading

As seen in Figure 1.1, the miniemulsion-solvent evaporation approach was used to create all of the PLGA nanoparticles. A previously optimized procedure was used to produce blank PLGA nanoparticles prior to AuNR encapsulation in our lab [34]. The system's surface characteristics and structural stability were assessed using the nanoparticles in the absence of photothermal agents. Dynamic light scattering (DLS) analyses revealed that the blank nanoparticles had an average hydrodynamic diameter of 220 nm and a polydispersity index (PDI) of 0.11, indicating a uniform size distribution (Table 4.1). This initial characterization served as a crucial baseline for assessing the following effects of AuNR loading on particle size, shape, and stability. In the literature, the hydrodynamic diameter of blank PLGA nanoparticles produced by using PVA generally varies between ∼92–258 nm [52],[54],[55]. The particles developed in this study (∼220 nm) are positioned toward the upper end of this range, which is often associated with higher encapsulation capacity due to increased core volume, while remaining within the biologically suitable size window for effective delivery.

Before the synthesis of drug and AuNR-loaded nanoparticles, we performed an optimization study for AuNR loading to determine the optimal concentration of gold nanorods (AuNR) for enhanced photothermal efficacy. Five PLGA nanoparticle formulations (PLGA-Au1 to PLGA-Au5) were developed by varying the AuNR concentrations while maintaining a constant PLGA content (Table 4.1). A thorough structural and optical analysis was conducted to evaluate the morphological integrity, the uniformity of AuNR distribution inside the nanoparticles, and their photothermal capabilities. Three main factors were taken into consideration when choosing the best formulation: AuNRs' successful incorporation into the polymeric matrix as opposed to their existence as free entities in the surrounding medium; their favorable physicochemical properties; and their uniform dispersion throughout the PLGA nanoparticles.

Visual inspection, STEM imaging, DLS measurements, and FTIR analysis combined facilitated the identification of the most promising formulation for future applications.

Table 4.1
Hydrodynamic dimensions and polydispersity index (PDI) values of PLGA nanoparticles containing gold nanorods at different loading ratios. Measurements were conducted using dynamic light scattering (DLS) in aqueous solutions prior to purification.

Sample Np	AuNR (% w/w of PLGA)	Size (nm)	PDI	Zeta Potential (mV)
$PLGA_{initial}$	0	220 ± 1	0.11 ± 0.01	-2.0 ± 0.7
PLGA-Au_1	5	293 ± 8	0.09 ± 0.02	-1.4 ± 0.5
PLGA-Au_2	10	287 ± 3	0.09 ± 0.10	-6.0 ± 0.2
PLGA-Au_3	14	213 ± 1	0.10 ± 0.01	-1.0 ± 0.7
PLGA-Au_4	27	297 ± 5	0.15 ± 0.03	-10.0 ± 0.2
PLGA-Au_5	41	228 ± 3	0.30 ± 0.02	-4.0 ± 0.4

PLGA-Au1 and PLGA-Au2 nanoparticles exhibited a marked increase in average hydrodynamic radius despite encapsulating relatively small amounts of gold nanorods compared to blank nanoparticles (Table 4.1). According to STEM imaging results, the PLGA-Au1 and PLGA-Au2 formulations showed an uneven distribution of gold nanorods (AuNRs) within the nanoparticles, likely due to the low initial AuNR content during encapsulation (Figure 4.1.A-B). Additionally, free AuNRs were visible outside the nanoparticles. In contrast, the PLGA-Au4 formulation, which incorporated more gold nanorods than PLGA-Au3, displayed a hydrodynamic radius of approximately 297 nm with a PDI of 0.15. The PLGA-Au3 sample, however, achieved a more desirable size of around 210 nm and a PDI value of 0.10 (Table 4.1). Although the PLGA-Au4 formulation had a higher gold nanorod input, it was also deemed unsuitable, as STEM images revealed an increased presence of unencapsulated AuNRs. In contrast, PLGA-Au3 exhibited a uniform AuNR distribution, favorable physicochemical characteristics, and successful encapsulation efficiency (Table 4.1,Figure 4.1).

In the highest loading attempt, where gold nanorods were added at 41% w/w relative to PLGA, aggregation occurred during synthesis. These aggregates were removed from the suspension via filtration and subsequently analyzed with Fourier-transform

infrared spectroscopy (FTIR) (Figure 4.2). The filtered suspension was further examined by STEM and DLS to assess remaining particles. STEM and FTIR findings confirmed that PLGA and AuNRs had interacted to form aggregates. The supernatant obtained after removing aggregated particles was further analyzed using STEM imaging and DLS measurements. DLS data revealed a relatively high PDI (0.30), attributed to particle aggregation, even though the average size remained within the target range. Due to this tendency toward aggregation, the PLGA-Au5 system was excluded from further testing.

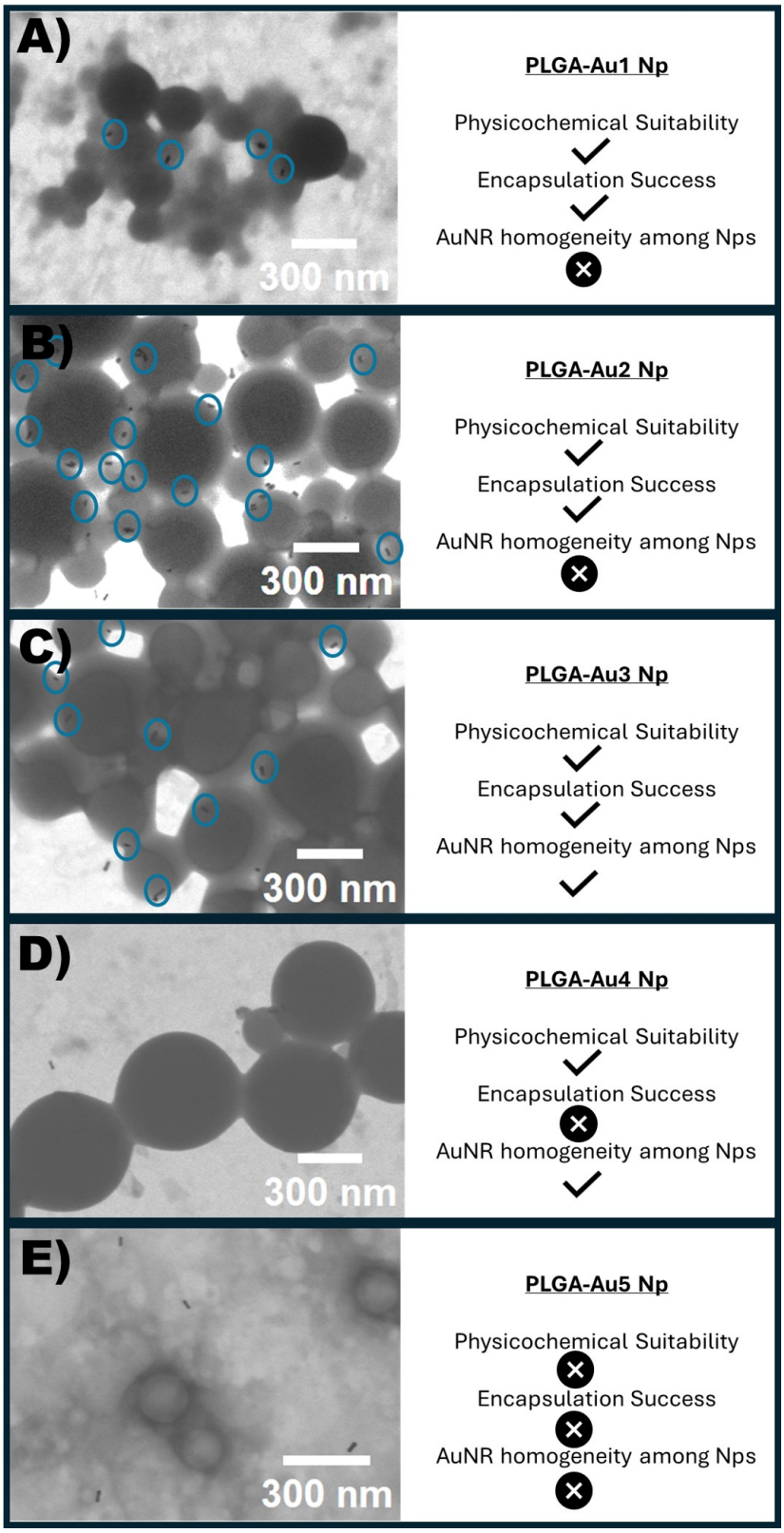

Figure 4.1 STEM images of PLGA nanoparticles encapsulating gold nanorods at varying loading ratios. (A) PLGA-Au1, (B) PLGA-Au2, (C) PLGA-Au3 (selected as optimal formulation), (D) PLGA-Au4, and (E) PLGA-Au5.

Among all the tested systems, PLGA-Au3 demonstrated the highest encapsulation efficiency and was selected as the optimal AuNR-loaded formulation. Before purification, optimum formulation was assessed to better reflect the actual entrapment performance of gold nanorods during synthesis. The optimized formulation (PLGA-Au3) was then centrifuged to remove impurities, yielding the purified version, referred to as PLGA-Au. This purification step was critical for eliminating toxic, CTAB-coated, non-encapsulated AuNRs. Moreover, since the formulation was intended for dual encapsulation with doxorubicin (DOX) in the subsequent steps, removing free DOX molecules and residual AuNRs after drug loading was essential to ensure accurate analysis. Hence, purification played a vital role in improving biocompatibility and establishing a robust and reproducible platform for drug incorporation and therapeutic evaluation.

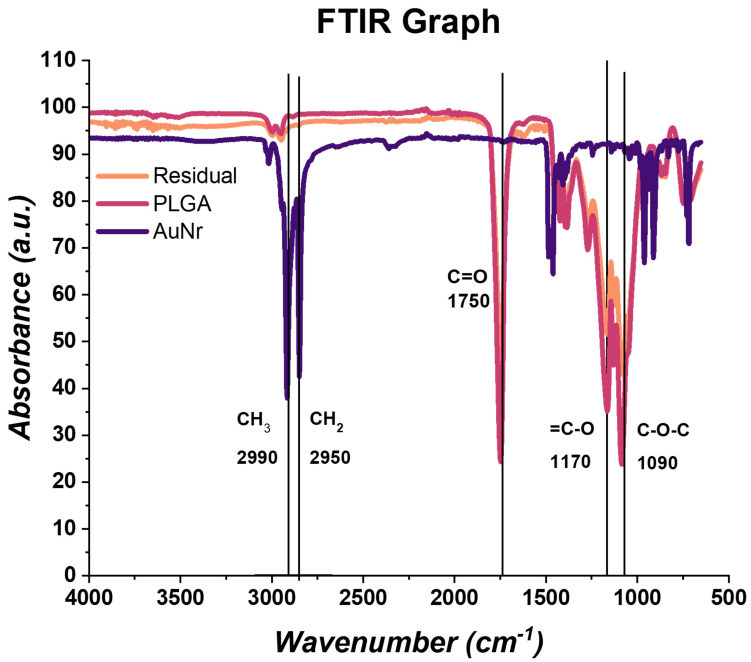

Figure 4.2 FTIR Spectrum of the residues precipitated in the synthesis of PLGA-Au5 encoded sample, PLGA and lyophilized AuNR.

4.2 Co-Encapsulation of AuNRs and DOX: Evaluation of Drug Release Behavior

Following DLS and STEM analyses, the PLGA–Au3 nanoparticle sample, identified as the optimal formulation, underwent two purification steps by centrifugation at 6000 rpm for 30 minutes each. The purified nanoparticles are hereafter referred to as PLGA-Au Np. After purification, the hydrodynamic radius of PLGA–Au Np increased slightly from approximately 213 nm to 221 nm, while the PDI decreased from 0.10 to 0.06. For consistency in comparison, the $PLGA_{initial}$ nanoparticles presented in Table 4.1 were also subjected to the same centrifugation protocol, and their characterizations were repeated after this purification step (referred as $PLGA_{purified}$. Even after multiple centrifugation steps, both PLGA and PLGA-Au nanoparticles maintained their structural integrity and monodisperse distribution, as confirmed by DLS measurements (Table 4.2) and STEM imaging (Figure 4.3). In this study, the purified optimum formulation (PLGA–Au Np) displayed a mean diameter of approximately 220 nm (Table 4.2) following centrifugation, indicating a smaller and more compact particle size compared to values commonly reported. Literature data show that the diameters of PLGA nanoparticles incorporating gold nanorods typically range from 350 nm to 500 nm, depending on the formulation and production method used [8],[56].

After successful incorporation of gold nanorods (AuNRs) into PLGA nanoparticles and the optimization of purification conditions (6000 rpm for 30 minutes, repeated twice), doxorubicin (DOX) was subsequently loaded into the nanoparticle system. The hydrodynamic radius of these DOX-encapsulated PLGA nanoparticles is larger (241 nm) than that of blank PLGA and PLGA-Au Np and similar to that of PLGA-Au-DOX Np (246 nm). To assess the morphological and physicochemical characteristics of the synthesized and purified nanoparticles, STEM imaging was carried out (Figure 4.3). The resulting images confirmed that blank PLGA nanoparticles, prepared using our previously optimized laboratory protocol, maintained their spherical shape, smooth surface, and uniform size distribution, consistent with earlier observations [52].

For accurate comparison, the initial PLGA nanoparticles presented in Table 4.1 were also purified using the same centrifugation parameters, and subsequent characterizations were performed on these purified particles (referred to as $PLGA_{purified}$). Additionally, gold nanorods synthesized based on the previously established protocol by Zengin et al. [34] exhibited well-defined rod-shaped morphology with an average length of 32.5 ± 3.9 nm and an average width of 10.1 ± 1.6 nm, corresponding to an aspect ratio of 3.2 ± 0.7 (n= 64). In STEM images of PLGA-Au and PLGA-Au-DOX formulations, gold nanorods were clearly visible within the polymer matrix, retaining their original shape. The sustained spherical morphology of the nanoparticles indicated that AuNRs were successfully integrated without compromising structural integrity. Moreover, the bare AuNRs, analyzed prior to nanoparticle synthesis, preserved their dimensions and morphology throughout the process, further confirming their stability and applicability for photothermal therapy.

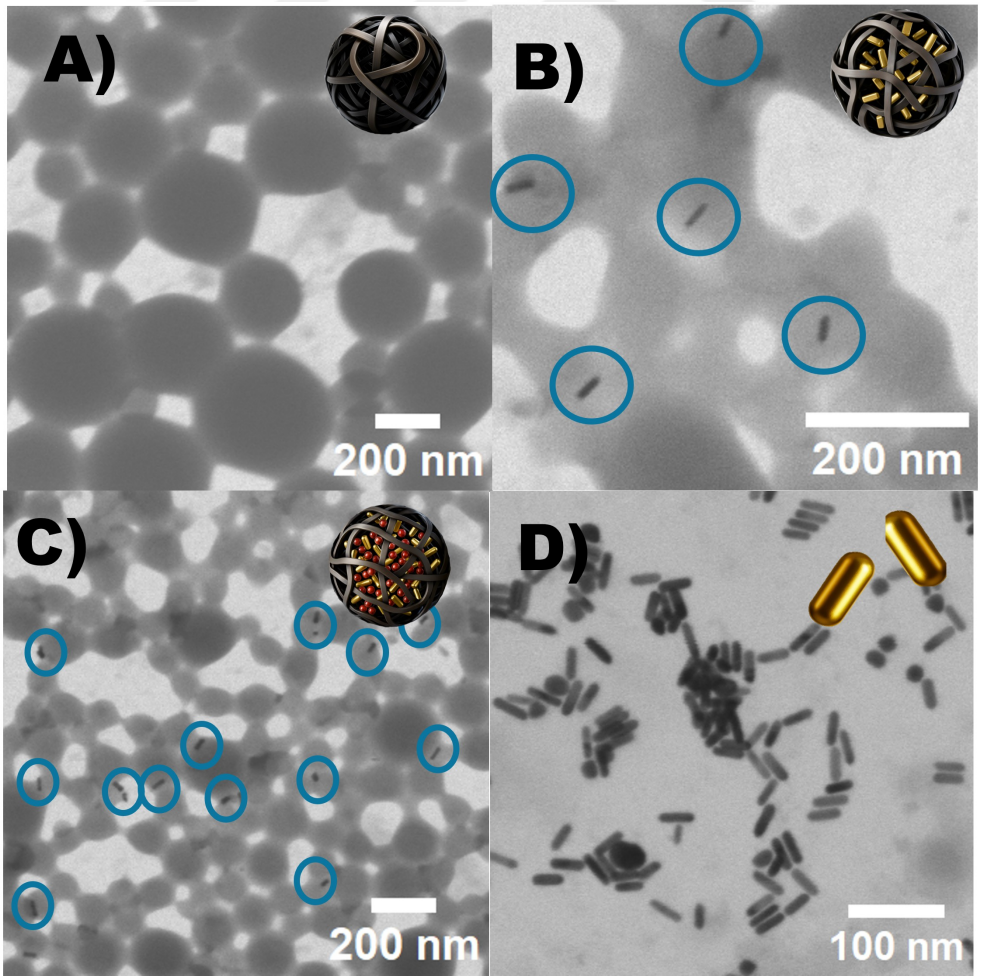

Figure 4.3 STEM images of the nanoparticles.

The hydrodynamic diameter, polydispersity index (PDI), and surface charge of the synthesized and purified nanoparticles were assessed using Dynamic Light Scattering (DLS) and Electrophoretic Light Scattering (ELS), as summarized in Table 4.2. All formulations exhibited mean particle sizes below 250 nm, a range considered favorable for cellular internalization and effective tumor accumulation via the enhanced permeability and retention (EPR) effect. Compared to blank PLGA nanoparticles, both PLGA-Au and PLGA-Au-DOX formulations showed a modest increase in particle size, attributed to the incorporation of gold nanorods and doxorubicin. Despite this increase, the particles maintained a uniform nanoscale distribution, as evidenced by PDI values below 0.1, indicating monodisperse populations and consistent formulation quality.

Table 4.2
Physicochemical properties of different nanoparticle formulations.

Sample	**Size (nm)**	**PDI**	**Zeta Potential (mV)**
$\text{PLGA}_{\text{purified}}$ Np	229 ± 1	0.09 ± 0.02	-1.4 ± 0.5
PLGA-Au Np	221 ± 2	0.06 ± 0.02	-2.4 ± 0.9
PLGA-DOX Np	241 ± 4	0.08 ± 0.02	-15.6 ± 1.3
PLGA-Au-DOX Np	246 ± 3	0.09 ± 0.02	-16.3 ± 1.2

Zeta potential measurements revealed that all nanoparticle formulations possessed slightly negative surface charges close to zero, attributed to the use of a non-ionic surfactant during synthesis. Despite their low zeta potential, colloidal stability was likely maintained through steric stabilization conferred by the adsorbed surfactant, consistent with previous findings [52],[57],[58].

To further characterize the system, thermogravimetric analysis (TGA) was performed to assess both the thermal stability and gold content of the PLGA-Au-DOX formulation (Figure 4.4). In the CTAB-coated gold nanorods (AuNR) sample, TGA revealed a residual mass of approximately 10.76%, which aligns well with literature-reported values of 12% for similarly structured AuNRs [59]. The observed high mass

loss was primarily due to the thermal decomposition of the CTAB coating, emphasizing the necessity of surface modification [34] or encapsulation into biocompatible materials ,as in this study, to mitigate CTAB-associated cytotoxicity.

For thermogravimetric analysis (TGA), the nanoparticle suspension was lyophilized after being arranged to an optimal level of 0.714 mg/mL. The actual concentration of the dried sample was found to be 1.275 mg/mL. Based on the 10.76% residual mass and an initial volume of 10 mL, the total amount of elemental gold in the sample was calculated to be 1.37 mg. As shown in the TGA thermogram (Figure 4.4), the PLGA-Au-DOX nanoparticle formulation exhibited a slight initial weight loss (∼0.88%) below 200 °C, attributed to the evaporation of moisture. The main degradation occurred above 200 °C, corresponding to the breakdown of the PLGA matrix, PVA and the encapsulated doxorubicin. At 800 °C, the final residue was 1.9%, confirming the presence of thermally stable gold nanorods. Given the dried sample's concentration of 3.44 mg/mL, the total encapsulated gold content in PLGA-Au-DOX was determined to be 0.66 mg, representing a 48% encapsulation efficiency relative to the initial 1.37 mg of pure gold. For comparison, a study by Amirishoar *et al.* reported an encapsulation efficiency of only 1.1%, since our formulation achieved approximately 1.8-fold higher gold content, highlighting the improved loading capacity achieved in this study [38].

Doxorubicin (DOX) loading was quantitatively assessed for both PLGA-DOX and PLGA-Au-DOX nanoparticle formulations. Each formulation was prepared in triplicate ($n = 3$) to ensure reproducibility. The PLGA-DOX nanoparticles demonstrated a drug loading concentration of 85 ± 22 μg/mL, whereas the PLGA-Au-DOX formulations exhibited a significantly lower concentration of 32 ± 4 μg/mL. These findings indicate that the incorporation of gold nanorods (AuNRs) into the polymeric matrix may compromise drug loading efficiency, potentially due to competition for encapsulation space or physicochemical interactions between DOX and AuNRs during nanoparticle formation. This observation is consistent with previous studies, which reported a decrease in DOX encapsulation efficiency when co-loaded with hydrophobic

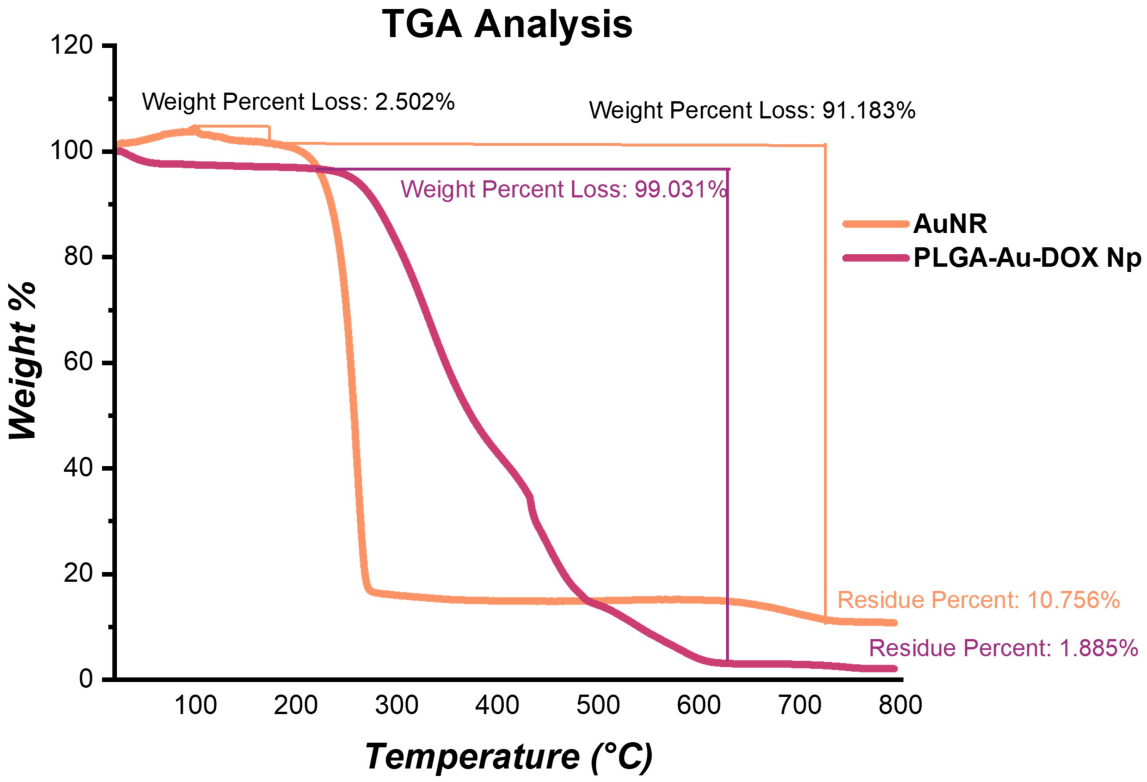

Figure 4.4 TGA analysis of the samples of PLGA-Au-DOX Np and AuNR.

AuNRs in PLGA-based systems [1]. In a multifunctional nanocomposite composed of PLGA, DOX, and AuNRs with a human serum albumin (HSA) coating, encapsulation efficiency dropped from 33.4% in DOX/PLGA nanoparticles to 30.4% and 23.0% in formulations with low and high AuNR content, respectively. Despite the reduction, DOX was still encapsulated at therapeutically relevant concentrations across all AuNR-loaded systems [1].

The *in vitro* release profiles of PLGA-DOX and PLGA-Au-DOX nanoparticles displayed a characteristic biphasic pattern, beginning with an initial burst release, followed by a sustained release plateau and eventual stabilization (Figure 4.5). This release behavior is consistent with prior studies on PLGA-based systems, where an early burst phase is commonly observed due to the nature of the polymer matrix [58]. In both formulations, a notable portion of doxorubicin was released within the first hour,

with minimal additional release in the following period. The similarity between the release curves suggests that the presence of gold nanorods did not markedly influence the passive diffusion of DOX from the PLGA matrix under the tested conditions.

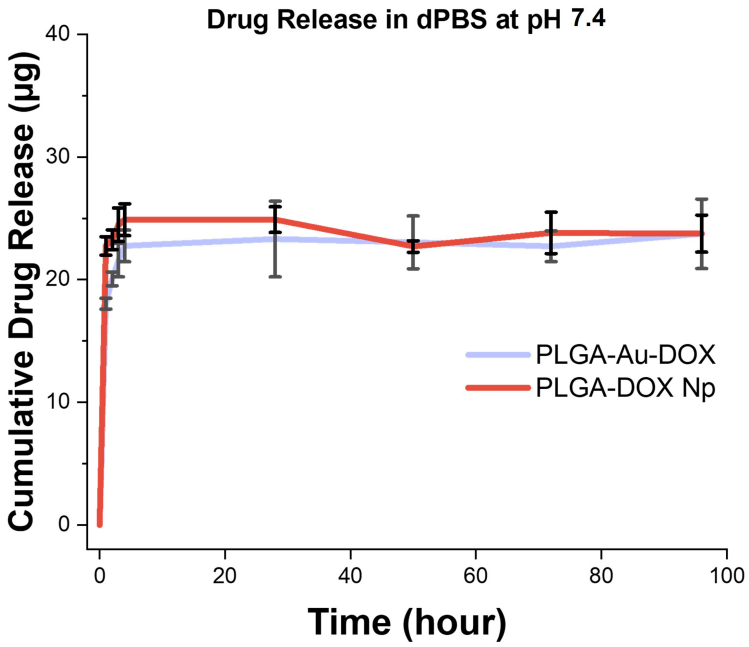

Figure 4.5 Cumulative drug release profiles of PLGA-DOX and PLGA-Au-DOX nanoparticles in DPBS at 37 °C.

Such a release profile aligns with previously reported data for acid-terminated PLGA nanoparticles. For instance, Betancourt et al. reported that acid-end capped PLGA nanoparticles (∼230 nm, $\zeta \approx -45$ mV) released 20–30% of encapsulated DOX within the first hour at pH 7.4, followed by a gradual release reaching 65–75% over 24 hours. In contrast, at pH 4.0, over 50% of DOX was released in the first hour, exceeding 90% within 12 hours—an effect attributed to polymer autocatalysis and the diminished ionic interaction between cationic DOX and deprotonated PLGA carboxyl groups [60]. Similarly, Wang et al. compared acid-terminated and ester-terminated PLGA microspheres loaded with doxycycline, finding that although acid-terminated formulations had lower encapsulation efficiency, they exhibited significantly faster release rates and earlier bulk erosion [50]. In contrast, ester-terminated systems retained over 50% of the drug even after 42 days, demonstrating a more prolonged release profile. Given that our formulation also utilized acid-terminated PLGA, the initial burst release we

observed aligns with the rapid early-phase drug diffusion reported in previous studies.

4.3 Stability Profile of AuNR and PLGA Nanoparticle Systems

To facilitate the potential clinical application of the developed photothermal nanoparticle system, extensive stability studies were performed under varying conditions. Specifically, long-term colloidal and structural stability was monitored over a 110-day period using two distinct centrifugation protocols designed to mimic practical storage and handling conditions. This comparative approach aimed to clarify how cumulative mechanical stress, introduced by repeated centrifugation, influences the structural and optical integrity of gold nanorods (AuNRs), both in their unencapsulated form and when embedded within PLGA nanoparticles.

The motivation for this investigation stemmed from the observation that AuNRs are subjected to multiple centrifugation steps throughout their synthesis and purification processes. Given that the complete formulation workflow includes four successive centrifugation cycles, including a final spin before encapsulation, it was essential to systematically assess how these repeated procedures may impact the colloidal stability of both free and encapsulated AuNRs.

While prior studies have provided only limited insights into the colloidal stability of PLGA-Au nanocomposites, our 110-day investigation, utilizing controlled stirring speeds (rpm) and a multi-step centrifugation protocol, offers the first long-term physical stability dataset in the literature. The results demonstrate that PLGA nanospheres successfully preserve the morphology of encapsulated gold nanorods (AuNRs) over extended periods, whereas uncoated AuNRs rapidly undergo aggregation and a loss of their characteristic longitudinal surface plasmon resonance (LSPR) features under identical conditions (Figure 4.6 and Figure 4.7).

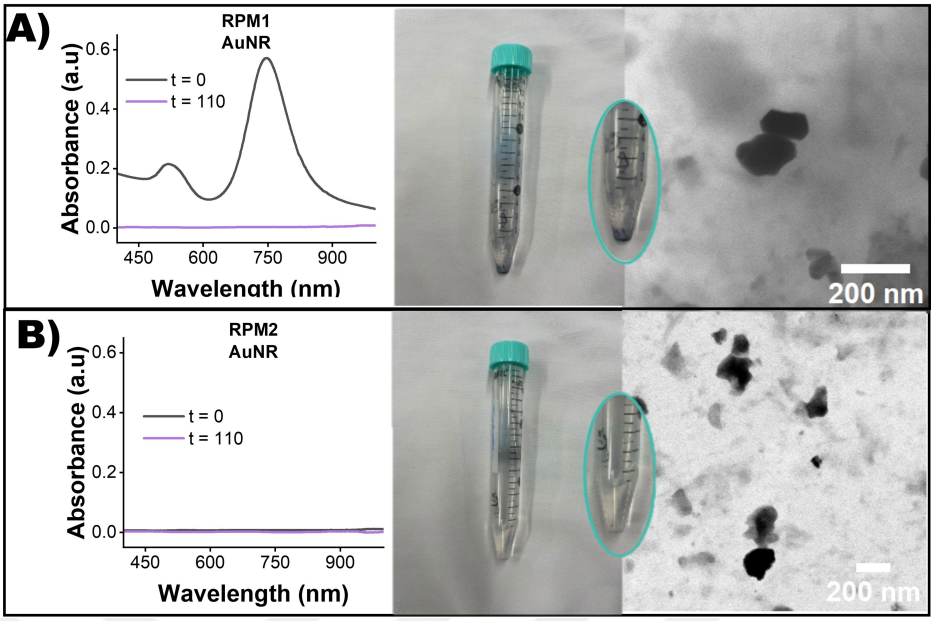

Figure 4.6 Morphological evaluation of unencapsulated AuNRs after different centrifugation protocols at t=0 and t=110 days, and STEM images at t=110 days for (A) RPM1 condition and (B) RPM2 condition.

Control experiments further revealed that unencapsulated AuNRs experienced rapid morphological deterioration during post-synthesis processing steps, as seen in both RPM1 and RPM2 protocols (Figure 4.6). In this study, two distinct centrifugation sequences were applied to AuNRs both before and after purification. The first protocol (RPM1) involved a two-step process: centrifugation at 4000 rpm followed by 12,000 rpm. The second, more rigorous protocol (RPM2), consisted of four consecutive spins as 4000 rpm, 12,000 rpm, 6000 rpm, and a final 6000 rpm cycle. These protocols were exclusively applied to free AuNRs and PLGA-Au nanoparticle formulations. The physicochemical outcomes of RPM1 are presented under the label PLGA-Au3 in Table 4.1, while results from RPM2 are reported as PLGA-Au Np in Table 4.2.

Following repeated centrifugation, the distinctive longitudinal LSPR band of the bare AuNRs completely vanished within 18 days (Figure 4.6.B), accompanied by visual evidence of aggregation in the form of dark precipitates at the bottom of storage tubes and amorphous agglomerates in STEM images. Notably, STEM analysis of centrifuged AuNRs revealed isotropic gold masses ranging from 80–300 nm in diam-

eter. These formations represent advanced rod-rod fusion stages, typically occurring after the depletion of the CTAB surface layer, a phenomenon well-documented in prior studies [61],[62]. The loss of the longitudinal LSPR band can be attributed not only to morphological deformation and aggregation but also to the gradual depletion of nanorods during successive washing steps, which ultimately leads to a decrease in optical density observed in the RPM2 protocol. In contrast, gold nanorods encapsulated within PLGA maintained their characteristic rod-like morphology and optical properties even after 110 days of storage under identical centrifugation conditions (Figure 4.7 and Figure 4.8).

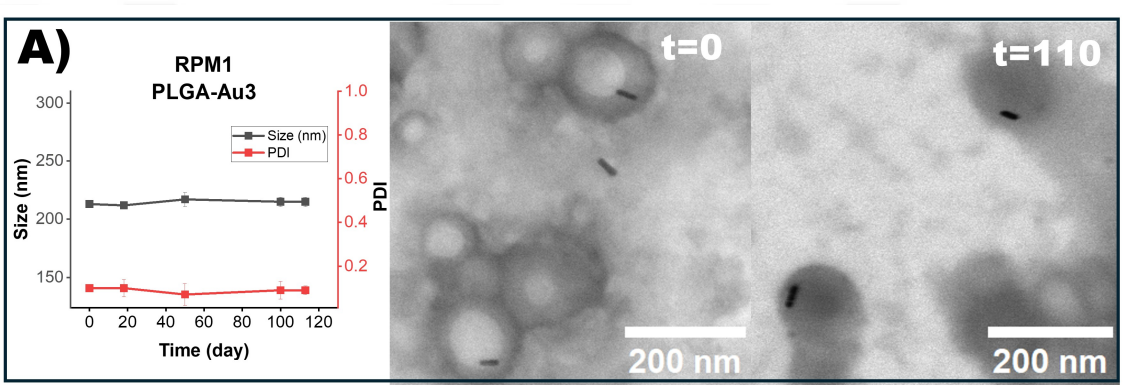

Figure 4.7 Stability analysis of AuNR encapsulated PLGA nanoparticles subjected to RPM1 centrifugation protocol. (A) Hydrodynamic size and polydispersity index (PDI) were monitored over a 110-day storage period by dynamic light scattering (DLS) , and morphological changes were visualized using STEM imaging at (B) day 0 ($t = 0$) and (C) day 110 ($t = 110$).

These results underscore the protective role of the PLGA matrix in preserving AuNR structure by preventing CTAB desorption, thereby maintaining colloidal stability throughout multiple washing and resuspension cycles (Figure 4.7 and Figure 4.8).

To assess the long-term colloidal and structural stability of PLGA nanoparticles under physiologically relevant conditions, samples were stored in buffer solutions at pH 7.4, 6.5, and 5.5 at 4 °C and monitored for over 300 days (Figure 4.9). The objective was to examine how varying pH and ionic strengths affect nanoparticle stability over time, particularly after the removal of excess surfactant and free polymer through a double centrifugation process. This approach enabled the use of purified resuspensions for stability evaluation and provided valuable insight into the behavior

of PLGA nanoparticles—the core component of our nanocarrier system—under conditions mimicking physiological and pathological environments.

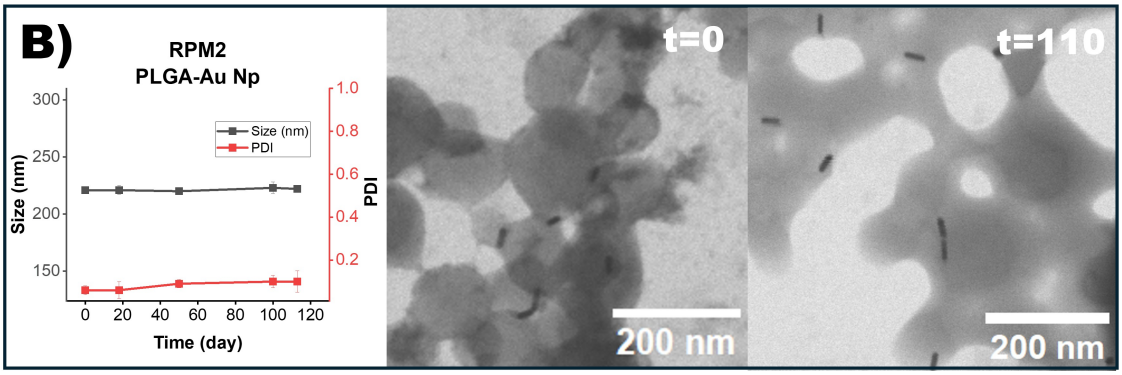

Figure 4.8 Stability analysis of AuNR encapsulated PLGA nanoparticles subjected to RPM2 centrifugation protocol. (A) Hydrodynamic size and polydispersity index (PDI) were monitored over a 110-day storage period by dynamic light scattering (DLS) , and morphological changes were visualized using STEM imaging at (B) day 0 ($t = 0$) and (C) day 110 ($t = 110$).

In this STB-Buffer protocol, nanoparticles underwent two centrifugation steps prior to buffer storage to eliminate unbound surfactants. Remarkably, the hydrodynamic diameter and polydispersity index (PDI) remained stable across all pH conditions throughout the 300-day period (Figure 4.9). This consistent size and distribution suggest that the PLGA matrix effectively preserves nanoparticle integrity even in mildly acidic environments (pH 6.5 and 5.5), which are relevant to tumor microenvironments and endosomal compartments.

Furthermore, the similarity in size and PDI before and after centrifugation indicates that while excess polyvinyl alcohol (PVA) is removed, the tightly adsorbed PVA remains bound to the nanoparticle surface, likely contributing to the observed long-term colloidal stability. Collectively, these results underscore the robustness of the miniemulsion-based synthesis method and confirm the suitability of the resulting PLGA nanoparticles for biomedical applications requiring extended stability, even after purification.

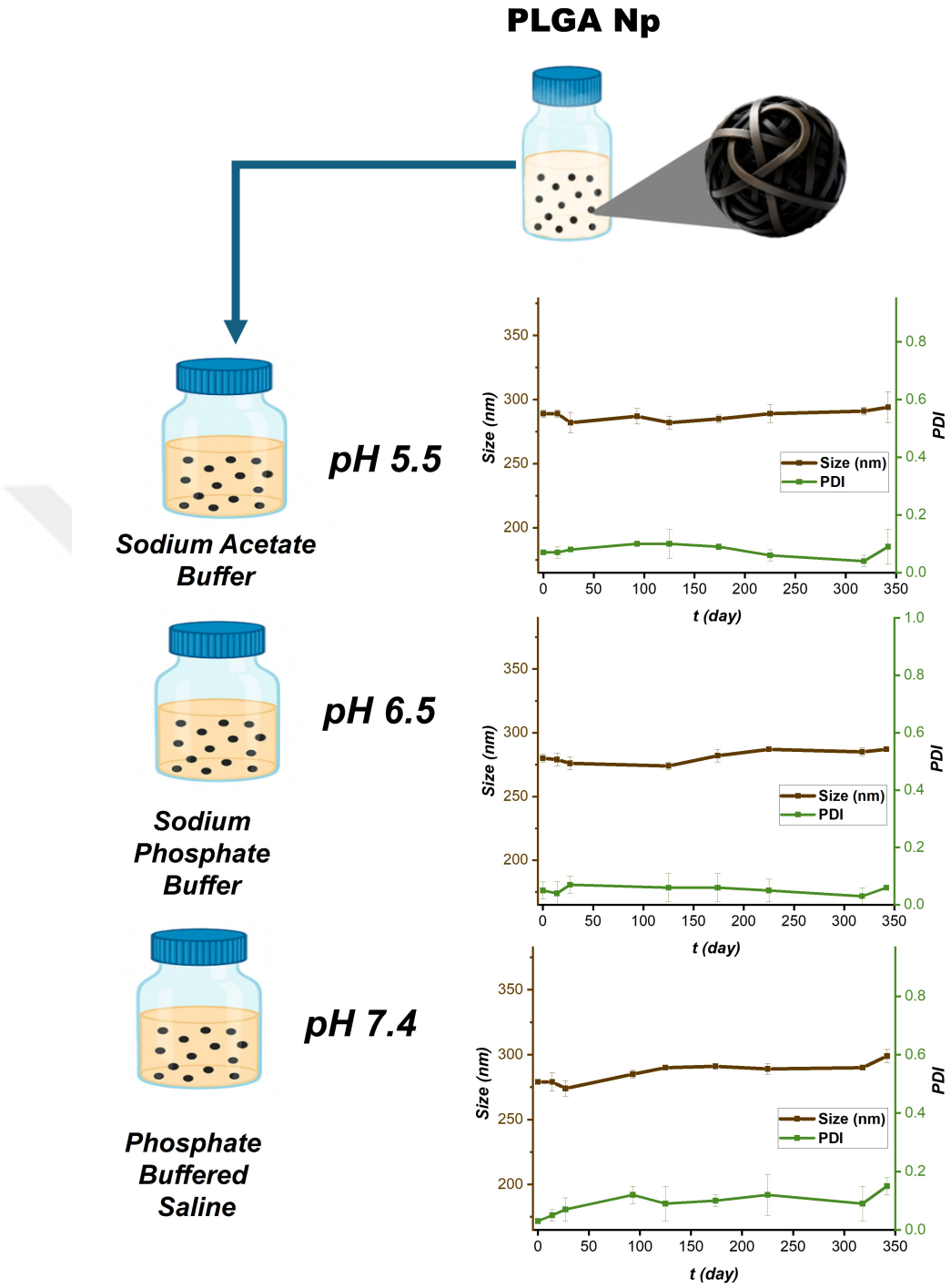

Figure 4.9 Blank PLGA nanoparticles were incubated in three buffer systems(pH 5.5, 6.5, and 7.4).

4.4 Laser-Induced Photothermal Behavior of the Nanoparticle System

Following the optimization of gold nanorod and doxorubicin encapsulation, laser irradiation experiments were conducted to verify the photothermal conversion efficiency of the formulation containing the optimal AuNR loading. Specifically, temperature elevations resulting from NIR-induced heating were measured for PLGA-Au and PLGA-Au-DOX nanoparticles and compared to blank PLGA nanoparticles (control) at varying power densities. For these measurements, 0.3 mL of each formulation was placed in centrifuge tubes and monitored using a thermal camera.

As shown in Figure 4.10, the encapsulation of gold nanorods within the PLGA matrix enabled effective and controllable heat generation upon NIR laser exposure. Notably, PLGA-Au-DOX nanoparticles exhibited a temperature rise of approximately 25 °C within 5 minutes under 808 nm laser irradiation at 1.0 W/cm^2, whereas blank PLGA nanoparticles showed minimal temperature change. A clear correlation was observed between power density and temperature increase for AuNR-loaded formulations (PLGA-Au and PLGA-Au-DOX), whereas no significant temperature shift occurred in PLGA-only controls across all tested power levels. As previously discussed, the gold content encapsulated in our nanoparticle formulation was compared with that reported by Amirishoar et al. [38]. According to the results, while their system exhibited a temperature increase of only 10 °C after 60 minutes of laser irradiation at 1 W/cm^2, our formulation achieved an approximate 25 °C rise within just 5 minutes under identical conditions. This substantial difference suggests a more efficient photothermal conversion in our system, likely attributable not only to differences in AuNR loading but also to additional formulation parameters; such as nanoparticle structure, dispersion stability, or polymer–nanorod interactions, which may collectively enhance heat generation efficiency.

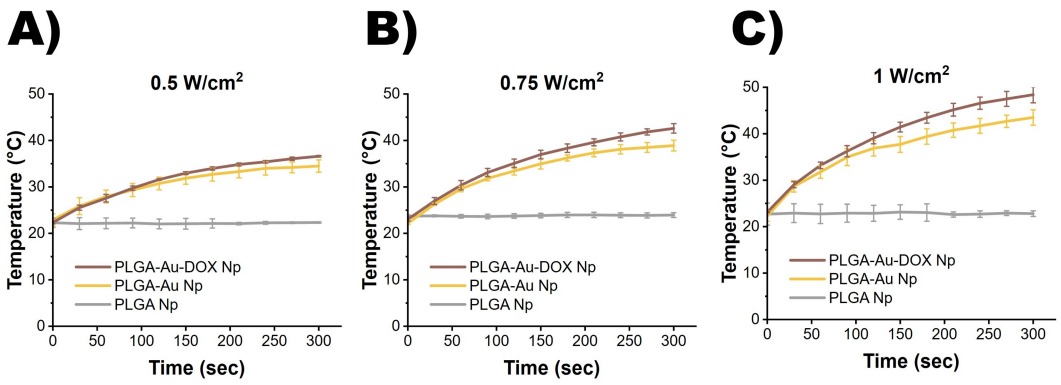

D)

Sample	ΔT (°C) 0.5 W/cm²	ΔT (°C) 0.75 W/cm²	ΔT (°C) 1 W/cm²
PLGA-Au Np	11.60 ± 0.70	16.70 ± 0.90	21.20 ± 1.60
PLGA-Au-DOX Np	14.30 ± 0.10	19.60 ± 1.30	25.30 ± 1.70

Figure 4.10 Photothermal response of PLGA-Au nanoparticles at constant volume under different laser power densities.

As presented in Figure 4.10.D, the temperature variations recorded for the blank PLGA nanoparticles across all three power densities were negligible, confirming their role as an effective control. This observation rules out any significant photothermal contribution from the polymer or residual PVA, thereby attributing the entire thermal effect to the presence of gold nanorods. Notably, the DOX-loaded formulation consistently produced a 2–3 °C higher temperature increase compared to its Au-only counterpart under identical laser irradiation conditions. This finding indicates that doxorubicin encapsulation does not hinder AuNR incorporation. Furthermore, temperature elevation in all AuNR-containing formulations showed a clear dependence on applied power density, reflecting a dose-responsive heating behavior.

4.5 Dual-Modality Treatment Outcomes: Cytotoxic and Photothermal Responses

Following confirmation of the favorable physicochemical characteristics of the nanoparticle formulations, stability assessments and photothermal performance tests were conducted. Based on the positive outcomes, further evaluations were carried out at the cellular level. The biocompatibility of both blank PLGA and gold-loaded PLGA (PLGA–Au) nanoparticles was assessed using the MTT cell viability assay on L929 mouse fibroblast cells (ATCC CCL-1), in accordance with ISO 10993-5:2020 guidelines (Figure 4.11).

For blank PLGA nanoparticles, no notable dose- or time-dependent cytotoxic effects were observed, indicating that the polymer matrix is biologically inert under the experimental conditions described previously. Similarly, PLGA nanoparticles encapsulating gold nanorods exhibited no concentration-dependent cytotoxicity. At the highest tested concentration of 150 μg/mL, PLGA–Au nanoparticles maintained approximately 79% cell viability after 24 hours and 72% after 48 hours of exposure. Blank PLGA nanoparticles demonstrated comparable results, with cell viabilities of approximately 63% at 24 hours and 80% at 48 hours. Importantly, all tested concentrations preserved $\geq$72% viability after 48 hours, exceeding the ISO-defined biocompatibility threshold of 70%. These findings confirm that both PLGA and PLGA–Au nanoparticles are well tolerated by L929 cells, even at elevated concentrations, supporting their suitability for further biomedical applications.

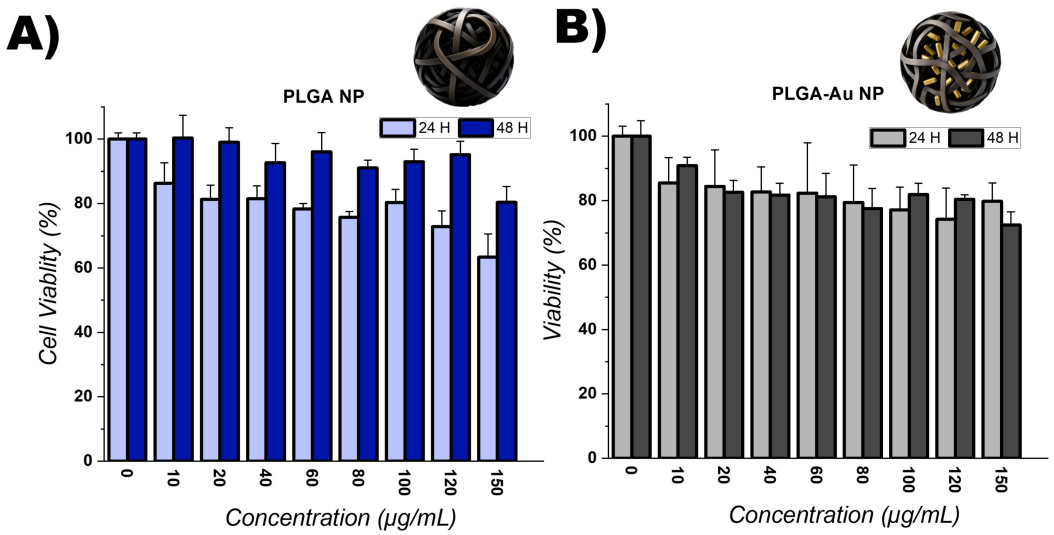

Figure 4.11 Cell viability on L929 cell line.

To ensure consistent experimental conditions across all treatment groups, nanoparticle and laser interaction studies were conducted using a single 96-well plate. This setup allowed for direct comparison between laser-irradiated and non-irradiated cells, while select wells were intentionally left empty to prevent unintended heat diffusion between neighboring wells.

PLGA-based nanoparticles were administered at concentrations of 150 and 250 μg/mL following a 24-hour cell attachment period. After an additional 24-hour incubation, the wells were gently washed, and fresh culture medium was added. Subsequently, designated wells were exposed to an 808 nm near-infrared (NIR) laser at 1W/cm^2 for 300 seconds, while control wells were kept under identical conditions without laser exposure. Cell viability was assessed 24 hours post-irradiation using the MTT assay (Figure 4.12), enabling evaluation of the photothermal effect on cell survival in the presence of PLGA-based nanoparticle formulations.

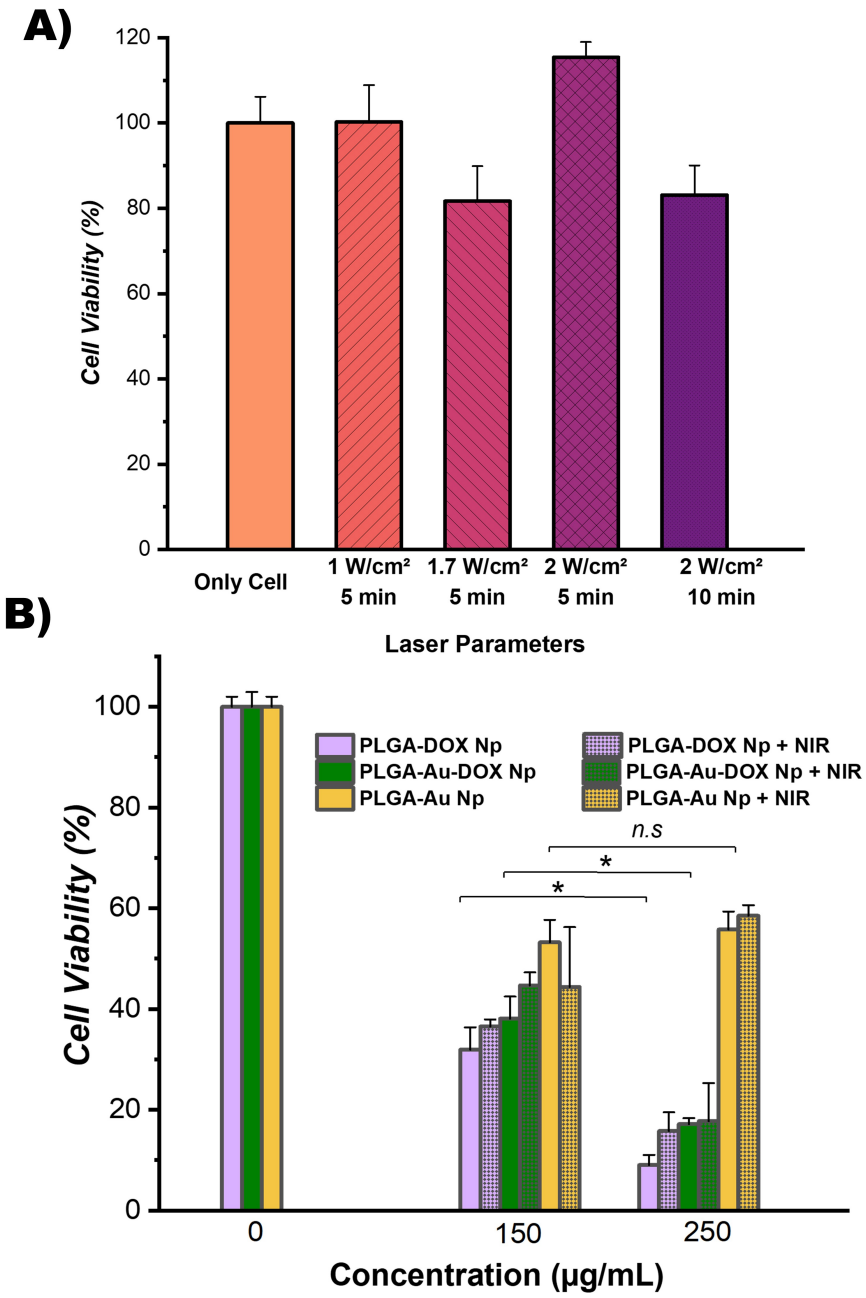

Figure 4.12 Cell viability after NIR irradiation of (A) only MCF-7 cell line and (B) nanoparticle containing MCF-7 cell line.

To independently determine the effects of laser irradiation without nanoparticle interference, MCF-7 cells were exposed to varying power densities and durations of NIR laser treatment (Figure 4.12A). Irradiation at 1 W/cm^2 for 5 min resulted in

no statistically significant change in cell viability compared to untreated controls ($p = 0.062$). Increasing the power to 1.7 W/cm^2 for 5 min reduced viability by approximately 18±8% ($p = 0.055$). A brief exposure at 2 W/cm^2 for 5 min produced a modest increase in the MTT signal ($p = 0.119$), whereas extending the same power to 10 min lowered viability to about $83 \pm 7\%$ ($p = 0.080$). Based on these results, the laser condition of 1 W/cm^2 for 5 min was chosen for subsequent experiments, as it caused the smallest deviation from the control group and did not lead to any significant change in cell viability.

To apply laser treatment to cells containing nanoparticles, all experimental groups were seeded on the same 96-well plate to ensure uniform conditions between laser-exposed and non-exposed cells. PLGA-based nanoparticles (150 and 250 μg/mL) were added following a 24 h attachment period. After 24 h of incubation, the wells were washed and replenished with fresh medium. Selected wells were irradiated with an 808 nm laser (1 W/cm^2, 300 s), while control wells remained under comparable ambient conditions without exposure. Cell viability was assessed using the MTT assay after an additional 24 h. At a concentration of 150 μg/mL, PLGA-DOX resulted in $32 \pm 4\%$ viability, whereas PLGA-DOX + NIR showed $37 \pm 1\%$, indicating a modest and statistically insignificant increase in cytotoxicity ($p > 0.05$). This slight improvement may arise from a combination of thermal effects and altered drug diffusion at this concentration. The negligible difference is likely due to the already high cytotoxicity of DOX at this dose, which may mask any additional thermal contribution in the absence of a photothermal agent.

When doxorubicin (DOX) was co-encapsulated with gold nanorods in the PLGA-Au-DOX formulation, a comparable trend to the PLGA-DOX system was observed. In the absence of laser exposure, the PLGA-Au-DOX group resulted in a cell viability of 38%, whereas laser-treated samples (PLGA-Au-DOX + NIR) showed slightly higher viability at 45%. This unexpected outcome suggests that photothermal heating at this dose may have modified drug release kinetics, potentially reducing DOX bioavailability and thereby diminishing cytotoxicity despite the presence of both AuNRs and DOX.

Notably, at a higher nanoparticle concentration (250 μg/mL), all DOX-containing formulations exhibited markedly greater cytotoxicity compared to their 150 μg/mL counterparts. For example, PLGA-DOX + NIR and PLGA-Au-DOX + NIR treatments resulted in cell viabilities of 16% and 18%, respectively. This concentration-dependent enhancement in therapeutic effect likely reflects increased drug availability and uptake, contributing to elevated cytotoxic stress. Collectively, these results affirm the chemotherapeutic potential of DOX-loaded PLGA nanoparticles and support their efficacy in delivering cytotoxic agents to cancer cells.

Additionally, gold-loaded nanoparticles subjected to NIR laser irradiation (PLGA-Au + NIR) led to a moderate increase in cell viability, 44% at 150 μg/mL and 58% at 250 μg/mL, which is likely attributable to photothermal effects alone, in the absence of chemotherapeutic agents. In a related study, 808 nm laser exposure at 2.5W/cm^2 for 10 minutes resulted in an unexpected increase in cell viability in MCF-7 breast cancer cells treated with both blank PLGA and folic acid-functionalized PLGA nanoparticles [38]. The authors suggested that this concentration-dependent proliferation could be due to the natural, biodegradable nature of the polymers, which may provide nutritive support and promote cellular growth.

Overall, the results indicate that, under the tested conditions, the cytotoxic impact of DOX-containing formulations substantially surpassed any additional effect from NIR irradiation. The marked reduction in cell viability at higher DOX concentrations reflects the dominant chemotherapeutic activity. Rather than being a drawback, this outcome emphasizes that the successful combination of photothermal and chemotherapeutic modalities depends on the precise tuning of laser settings and nanoparticle architecture. It also implies that once a certain level of chemotherapeutic potency is reached, potential photothermal contributions may become less apparent. These observations provide valuable guidance for designing combination treatment strategies under physiologically relevant settings and for developing more efficient *in vivo* applications.

5. CONCLUSIONS AND OUTLOOK

5.1 Conclusions

This study focuses on the physicochemical characteristics, stability, photothermal potential, and biological performance of a multifunctional nanoparticle system made of poly(lactic-co-glycolic acid) (PLGA), gold nanorods (AuNRs), and the chemotherapeutic agent doxorubicin (DOX). It underscores the vital significance of nanoparticle composition and the optimization of laser parameters for the effective design of integrated photothermal-chemotherapeutic systems.

This comprehensive study has brought to light the following important findings and conclusions:

1. Acid-terminated PLGA nanoparticles synthesized via the miniemulsion method exhibited excellent physicochemical properties, demonstrating suitability for further formulation steps.

2. The mass ratio of gold nanorods (AuNRs) to PLGA plays a critical role in achieving efficient encapsulation. When the AuNR content exceeds a certain threshold relative to the polymer mass, particle aggregation and precipitation are observed in the system. This finding provides a valuable indication for determining the maximum AuNR loading capacity within the PLGA matrix.

3. TGA analysis verified that gold nanorods (AuNRs) were successfully encapsulated into the PLGA matrix, with an encapsulation efficiency of roughly 47%. This outcome is encouraging for advanced theranostic applications.

4. Doxorubicin (DOX) was effectively co-encapsulated with AuNRs in PLGA nanoparticles, resulting in particles with appropriate size, polydispersity index (PDI), and colloidal stability for biological applications.

5. When the DOX encapsulation efficiency in PLGA-Au-DOX and PLGA-DOX was examined, it was determined that there was more drug in the formulation containing only DOX.

6. *In vitro* release studies confirmed the characteristic sustained release profile of acid-terminated PLGA, with no significant alteration due to AuNR incorporation.

7. To the best of our knowledge, this is the first work to show that mechanical stress and the encapsulation state of AuNRs have a major impact on their long-term structural and optical stability over a period of 110 days. Encapsulation in PLGA Nps significantly inhibited aggregation and preserved LSPR integrity throughout repeated centrifugation.

8. PLGA-Au and PLGA-Au-DOX nanoparticles showed efficient photothermal conversion under NIR laser exposure, PLGA-Au-DOX nanoparticles generate temperature increases of up to 25 °C at 1W/cm^2, without affecting the polymer-only control group, confirming that the effect is entirely AuNR-driven.

9. Cytotoxicity experiments conducted on L929 fibroblasts indicated that both PLGA and PLGA-Au nanoparticles exhibit biocompatibility, even at elevated concentrations, surpassing ISO 10993-5 viability standards.

10. Photothermal therapy experiments on MCF-7 cancer cells revealed no synergistic effect between laser exposure and DOX treatment at tested conditions, while the cytotoxic response remained primarily concentration-dependent.

11. These findings collectively underscore the need of precise optimization of laser parameters and formulation design for future combined therapeutic techniques, and highlight the importance of assessing systems under physiologically relevant conditions for effective clinical translation.

12. A year-long investigation on colloidal stability was performed by keeping PLGA nanoparticles in buffer solutions at pH levels of 7.4, 6.5, and 5.5 at 4 °C to replicate physiologically relevant conditions. Following the elimination of excess surfactant using centrifugation, the purified nanoparticle suspensions exhibited stable hydrodynamic diameter and polydispersity index (PDI) values for a duration of

342 days. This discovery illustrates the exceptional structural stability of PLGA nanoparticles generated via miniemulsion and their appropriateness for prolonged storage under diverse pH settings, including those that replicate tumor microenvironments or endosomal compartments.

5.2 Outlook

Taken together, these findings suggest that no synergistic interaction was observed between NIR-induced photothermal therapy and chemotherapy under the tested conditions. Instead, the cytotoxicity of DOX-containing formulations appeared to increase primarily in a dose-dependent manner, indicating that the chemotherapeutic effect outweighed any additive or synergistic contribution from the photothermal component. These observations underscore the importance of meticulously optimizing both laser parameters and nanoparticle composition when designing combination therapies. Furthermore, they highlight the need to evaluate such systems under physiologically relevant, realistic conditions to ensure translational applicability in future *in vivo* studies.

APPENDIX A. SUPPLEMENTARY FIGURES

A.1 Calibration Curves

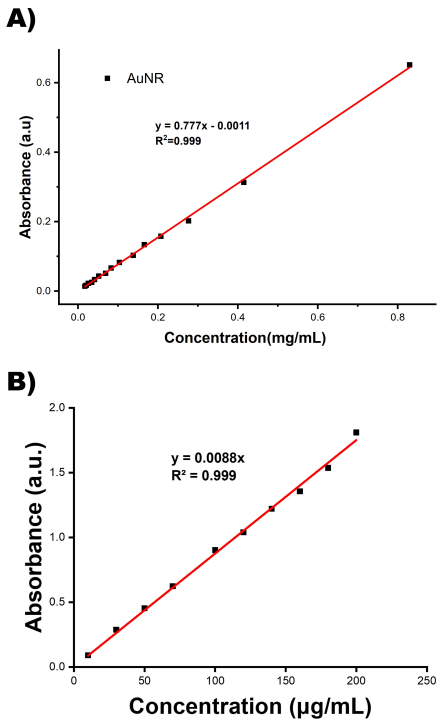

Figure A.1 A) Standard curve of AuNR in water and B)doxorubicin in Dpbs.

REFERENCES

1. Chuang, C. C., C. C. Cheng, P. Y. Chen, C. Lo, Y. N. Chen, M. H. Shih, and C. W. Chang, "Gold nanorod-encapsulated biodegradable polymeric matrix for combined photothermal and chemo-cancer therapy," *International Journal of Nanomedicine*, Vol. 14, pp. 181–193, 2018.

2. Wang, H., Y. Zhao, Y. Wu, Y. L. Hu, K. Nan, G. Nie, and H. Chen, "Enhanced anti-tumor efficacy by co-delivery of doxorubicin and paclitaxel with amphiphilic methoxy PEG-PLGA copolymer nanoparticles," *Biomaterials*, Vol. 32, no. 32, pp. 8281–8290, 2011.

3. Park, H., J. Yang, J. Lee, S. Haam, I.-H. Choi, and K.-H. Yoo, "Multifunctional nanoparticles for combined doxorubicin and photothermal treatments," *ACS Nano*, Vol. 3, no. 10, pp. 2919–2926, 2009.

4. Hribar, K. C., M. H. Lee, D. Lee, and J. A. Burdick, "Enhanced release of small molecules from near-infrared light responsive polymer-nanorod composites," *ACS Nano*, Vol. 5, no. 4, pp. 2948–2956, 2011.

5. Aioub, M., S. R. Panikkanvalappil, and M. A. El-Sayed, "Platinum-coated gold nanorods: Efficient reactive oxygen scavengers that prevent oxidative damage toward healthy, untreated cells during plasmonic photothermal therapy," *ACS Nano*, Vol. 11, no. 1, pp. 579–586, 2017.

6. Darwish, W. M. A., and N. A. Bayoumi, "Gold nanorod-loaded (PLGA-PEG) nanocapsules as near-infrared controlled release model of anticancer therapeutics," *Lasers in Medical Science*, Vol. 35, no. 8, pp. 1729–1740, 2020.

7. Liu, G., and K. McEnnis, "Glass transition temperature of PLGA particles and the influence on drug delivery applications," *Polymers*, Vol. 14, no. 5, p. 993, 2022.

8. Chu, C.-H., Y.-C. Wang, L.-A. Tai, L.-C. Wu, and C.-S. Yang, "Surface deformation of gold nanorod-loaded poly(dl-lactide-co-glycolide) nanoparticles after near infrared irradiation: an active and controllable drug release system," *Journal of Materials Chemistry*, Vol. 20, no. 16, pp. 3260–3264, 2010.

9. Gadag, S., S. Sinha, Y. Nayak, S. Garg, and U. Y. Nayak, "Combination therapy and nanoparticulate systems: Smart approaches for the effective treatment of breast cancer," *Pharmaceutics*, Vol. 12, no. 6, p. 524, 2020.

10. Xiong, X., L. W. Zheng, Y. Ding, *et al.*, "Breast cancer: pathogenesis and treatments," *Signal Transduction and Targeted Therapy*, Vol. 10, p. 49, 2025.

11. Singh, A., R. Mishra, and A. Mazumder, "Breast cancer and its therapeutic targets: A comprehensive review," *Chemical Biology & Drug Design*, Vol. 103, no. 1, p. e14384, 2024.

12. Alamdari, S. G., M. Amini, N. Jalilzadeh, B. Baradaran, R. Mohammadzadeh, A. Mokhtarzadeh, and F. Oroojalian, "Recent advances in nanoparticle-based photothermal therapy for breast cancer," *Journal of Controlled Release*, Vol. 349, pp. 269–303, 2022.

13. Agostinetto, E., J. Gligorov, and M. Piccart, "Systemic therapy for early-stage breast cancer: learning from the past to build the future," *Nature Reviews Clinical Oncology*, Vol. 19, no. 12, pp. 763–774, 2022.

14. Siddiqui, S. N., M. F. Haider, and M. A. Rahman, "Innovative approaches in breast cancer therapy: repurposing nanocarriers for enhanced outcomes," *Naunyn-Schmiedeberg's Archives of Pharmacology*, 2025.

15. Tommasi, C., R. Balsano, M. Corianò, B. Pellegrino, G. Saba, F. Bardanzellu, N. Denaro, M. Ramundo, I. Toma, A. Fusaro, S. Martella, M. M. Aiello, M. Scartozzi, A. Musolino, and C. Solinas, "Long-term effects of breast cancer therapy and care: Calm after the storm?," *Journal of Clinical Medicine*, Vol. 11, no. 23, p. 7239, 2022.

16. Wu, L., C. He, T. Zhao, T. Li, H. Xu, J. Wen, X. Xu, and L. Gao, "Diagnosis and treatment status of inoperable locally advanced breast cancer and the application value of inorganic nanomaterials," *Journal of Nanobiotechnology*, Vol. 22, no. 1, p. 366, 2024.

17. Gao, L., F. Meng, Z. Yang, M. Lafuente-Merchan, L. M. Fernández, Y. Cao, K. Kusamori, M. Nishikawa, S. Itakura, J. Chen, X. Huang, D. Ouyang, O. Riester, H. P. Deigner, H. Lai, J. L. Pedraz, M. Ramalingam, and Y. Cai, "Nano-drug delivery system for the treatment of multidrug-resistant breast cancer: Current status and future perspectives," *Biomedicine & Pharmacotherapy*, Vol. 179, p. 117327, 2024.

18. Zhang, L., W. Chen, S. Liu, and C. Chen, "Targeting breast cancer stem cells," *International Journal of Biological Sciences*, Vol. 19, no. 2, pp. 552–570, 2023.

19. Barathan, M., K. M. Vellasamy, V. Mariappan, G. Venkatraman, and J. Vadivelu, "Naturally occurring phytochemicals to target breast cancer cell signaling," *Applied Biochemistry and Biotechnology*, Vol. 196, no. 7, pp. 4644–4660, 2024.

20. Shukla, N., B. Singh, H.-J. Kim, M.-H. Park, and K. Kim, "Combinational chemotherapy and photothermal therapy using a gold nanorod platform for cancer treatment," *Particle & Particle Systems Characterization*, Vol. 37, no. 7, p. 2000099, 2020.

21. Núñez, C., J. L. Capelo, G. Igrejas, A. Alfonso, L. M. Botana, and C. Lodeiro, "An overview of the effective combination therapies for the treatment of breast cancer," *Biomaterials*, Vol. 97, pp. 34–50, 2016.

22. Yi, J., L. Liu, W. Gao, J. Zeng, Y. Chen, E. Pang, M. Lan, and C. Yu, "Advances and perspectives in phototherapy-based combination therapy for cancer treatment," *Journal of Materials Chemistry B*, Vol. 12, no. 26, pp. 6285–6304, 2024.

23. Wang, L., D. Li, Y. Hao, M. Niu, Y. Hu, H. Zhao, J. Chang, Z. Zhang, and Y. Zhang, "Gold nanorod-based poly(lactic-co-glycolic acid) with manganese dioxide core-shell structured multifunctional nanoplatform for cancer theranostic applications," *International Journal of Nanomedicine*, Vol. 12, pp. 3059–3075, 2017.

24. Zhong, Y., C. Wang, L. Cheng, F. Meng, Z. Zhong, and Z. Liu, "Gold nanorod-cored biodegradable micelles as a robust and remotely controllable doxorubicin release system for potent inhibition of drug-sensitive and -resistant cancer cells," *Biomacromolecules*, Vol. 14, no. 7, pp. 2411–2419, 2013.

25. Al-Hetty, H. R. A. K., A. T. Jalil, M. W. Alghazali, *et al.*, "Nanomaterials for combination cancer photothermal therapy," *Emergent Materials*, Vol. 6, pp. 425–438, 2023.

26. Sun, M., Y. Duan, Y. Ma, and Q. Zhang, "Cancer cell-erythrocyte hybrid membrane coated gold nanocages for near infrared light-activated photothermal/radio/chemotherapy of breast cancer," *International Journal of Nanomedicine*, Vol. 15, pp. 6749–6760, 2020.

27. Xing, Y., T. Kang, X. Luo, J. Zhu, P. Wu, and C. Cai, "Coral-shaped au nanostructures for selective apoptosis induction during photothermal therapy," *Journal of Materials Chemistry B*, 2019.

28. Li, J., S. Wang, F. Fontana, C. Tapeinos, M. A. Shahbazi, H. Han, and H. A. Santos, "Nanoparticles-based phototherapy systems for cancer treatment: Current status and clinical potential," *Bioactive Materials*, Vol. 23, pp. 471–507, 2022.

29. Beniwal, N., A. Verma, C. L. Putta, and A. K. Rengan, "Recent trends in bio-nanomaterials and non-invasive combinatorial approaches of photothermal therapy against cancer," *Nanotheranostics*, Vol. 8, no. 2, pp. 219–238, 2024.

30. Yang, S., L. Palanikumar, S. Jeong, K. Kim, J. Lee, E. Jeoung, and M.-H. Park, "Synergistic effect of photothermal therapy and chemotherapy using camptothecin-conjugated gold nanorods," *Particle & Particle Systems Characterization*, Vol. 35, no. 2, p. 1700307, 2017.

31. Pattani, V. P., J. Shah, A. Atalis, *et al.*, "Role of apoptosis and necrosis in cell death induced by nanoparticle-mediated photothermal therapy," *Journal of Nanoparticle Research*, Vol. 17, p. 20, 2015.

32. Duan, Q., M. Yang, B. Zhang, Y. Li, L. Li, J. Wang, W. Zhang, and S. Sang, "Gold nanoclusters modified mesoporous silica coated gold nanorods: Enhanced photothermal properties and fluorescence imaging," *Journal of Photochemistry and Photobiology B: Biology*, Vol. 215, p. 112111, 2021.

33. Liu, Y., M. Xu, Q. Chen, G. Guan, W. Hu, X. Zhao, M. Qiao, H. Hu, Y. Liang, H. Zhu, and D. Chen, "Gold nanorods/mesoporous silica-based nanocomposite as theranostic agents for targeting near-infrared imaging and photothermal therapy induced with laser," *International Journal of Nanomedicine*, Vol. 10, pp. 4747–4761, 2015.

34. Zengin, Y., D. Kelle, and B. Iyisan, "Design of biopolymer-coated gold nanorods as biorelevant photothermal agents," *Macromolecular Rapid Communications*, Vol. 45, no. 24, p. e2400497, 2024.

35. Chauhan, D., R. Prasad, J. Devrukhkar, K. Selvaraj, and R. Srivastava, "Disintegrable NIR light triggered gold nanorods supported liposomal nanohybrids for cancer theranostics," *Bioconjugate Chemistry*, Vol. 29, no. 5, pp. 1510–1518, 2018.

36. Alkilany, A. M., L. B. Thompson, S. P. Boulos, P. N. Sisco, and C. J. Murphy, "Gold nanorods: their potential for photothermal therapeutics and drug delivery, tempered by the complexity of their biological interactions," *Advanced Drug Delivery Reviews*, Vol. 64, no. 2, pp. 190–199, 2012.

37. Choi, W. I., A. Sahu, Y. H. Kim, and G. Tae, "Photothermal cancer therapy and imaging based on gold nanorods," *Annals of Biomedical Engineering*, Vol. 40, no. 2, pp. 534–546, 2012.

38. Amirishoar, M., S. Noori, J. Mohammadnejad, M. Rajabi Bazl, and A. Narmani, "Design and fabrication of folic acid-conjugated and gold-loaded poly (lactic-co-glycolic acid) biopolymers for suppression of breast cancer cell survival combining photothermal and photodynamic therapy," *Journal of Drug Delivery Science and Technology*, Vol. 83, p. 104266, 2023.

39. Tonbul, H., and G. Ultav, "Improving the doxorubicin loading to PLGA nanoparticles with TOPSIS-Based taguchi design approach: Effect of the water phase," *Journal of Pharmaceutical Innovation*, Vol. 19, p. 58, 2024.

40. Tsai, L. H., C. H. Yen, H. Y. Hsieh, and T. H. Young, "Doxorubicin loaded PLGA nanoparticle with cationic/anionic polyelectrolyte decoration: Characterization, and its therapeutic potency," *Polymers*, Vol. 13, no. 5, p. 693, 2021.

41. Bisht, A., D. Avinash, K. K. Sahu, P. Patel, G. Das Gupta, and B. D. Kurmi, "A comprehensive review on doxorubicin: mechanisms, toxicity, clinical trials, combination therapies and nanoformulations in breast cancer," *Drug Delivery and Translational Research*, Vol. 15, no. 1, pp. 102–133, 2025.

42. Singh, B., N. Shukla, J. Kim, K. Kim, and M.-H. Park, "Stimuli-responsive nanofibers containing gold nanorods for on-demand drug delivery platforms," *Pharmaceutics*, Vol. 13, no. 8, p. 1319, 2021.

43. Cardoso, V. M. d. O., *et al.*, "Stimuli-responsive polymeric nanoparticles as controlled drug delivery systems," in *Stimuli-Responsive Nanocarriers* (Gajbhiye, V., K. R. Gajbhiye, and S. Hong, eds.), pp. 87–117, Academic Press, 2022.

44. Danhier, F., E. Ansorena, J. M. Silva, R. Coco, A. Le Breton, and V. Préat, "PLGA-based nanoparticles: an overview of biomedical applications," *Journal of Controlled Release*, Vol. 161, no. 2, pp. 505–522, 2012.

45. Begines, B., T. Ortiz, M. Pérez-Aranda, G. Martínez, M. Merinero, F. Argüelles-Arias, and A. Alcudia, "Polymeric nanoparticles for drug delivery: Recent developments and future prospects," *Nanomaterials (Basel, Switzerland)*, Vol. 10, no. 7, p. 1403, 2020.

46. Lu, Y., D. Cheng, B. Niu, X. Wang, X. Wu, and A. Wang, "Properties of poly (lactic-co-glycolic acid) and progress of poly (lactic-co-glycolic acid)-based biodegradable materials in biomedical research," *Pharmaceuticals*, Vol. 16, no. 3, p. 454, 2023.

47. Bhardwaj, H., and R. K. Jangde, "Current updated review on preparation of polymeric nanoparticles for drug delivery and biomedical applications," *Next Nanotechnology*, Vol. 2, p. 100013, 2023.

48. Alsaab, H. O., F. D. Alharbi, A. S. Alhibs, N. B. Alanazi, B. Y. Alshehri, M. A. Saleh, F. S. Alshehri, M. A. Algarni, T. Almugaiteeb, M. N. Uddin, and R. M. Alzhrani, "PLGA-Based nanomedicine: History of advancement and development in clinical applications of multiple diseases," *Pharmaceutics*, Vol. 14, no. 12, p. 2728, 2022.

49. Kapoor, D. N., A. Bhatia, R. Kaur, R. Sharma, G. Kaur, and S. Dhawan, "PLGA: a unique polymer for drug delivery," *Therapeutic Delivery*, Vol. 6, no. 1, pp. 41–58, 2015.

50. Wang, J., L. Helder, J. Shao, J. A. Jansen, M. Yang, and F. Yang, "Encapsulation and release of doxycycline from electrospray-generated PLGA microspheres: Effect of polymer end groups," *International Journal of Pharmaceutics*, Vol. 564, pp. 1–9, 2019.

51. Martins, C., F. Sousa, F. AraÃºjo, and B. Sarmento, "Functionalizing PLGA and PLGA derivatives for drug delivery and tissue regeneration applications," *Advanced Healthcare Materials*, Vol. 7, no. 1, p. 1701035, 2018.

52. Kelle, D., K. R. Speth, M. Martínez-Negro, V. Mailänder, K. Landfester, and B. Iyisan, "Effect of protein corona on drug release behavior of PLGA nanoparticles," *European Journal of Pharmaceutics and Biopharmaceutics*, Vol. 207, p. 114611, 2025.

53. Schneider, C. A., W. S. Rasband, and K. W. Eliceiri, "NIH image to ImageJ: 25 years of image analysis," *Nature Methods*, Vol. 9, no. 7, pp. 671–675, 2012.

54. Hernández-Giottonini, K. Y., R. J. Rodríguez-Córdova, C. A. Gutiérrez-Valenzuela, O. Peñuñuri-Miranda, P. Zavala-Rivera, P. Guerrero-Germán, and A. Lucero-Acuña, "PLGA nanoparticle preparations by emulsification and nanoprecipitation techniques: effects of formulation parameters," *RSC Adv.*, Vol. 10, pp. 4218–4231, 2020.

55. Cooper, D. L., and S. Harirforoosh, "Design and optimization of PLGA-based diclofenac loaded nanoparticles," *PloS one*, Vol. 9, no. 1, p. e87326, 2014.

56. Wang, Y., M. Pastenak, Z. Wang, and M. Kolios, "Photoacoustic detection of cancer cells using targeted gold nanorod loaded PLGA nanoparticles," in *2017 IEEE International Ultrasonics Symposium (IUS)*, pp. 1–4, 2017.

57. Suzuki, T., A. Sasai, H. Tsujimoto, T. Yasunaga, N. Ogawa, and H. Yamamoto, "Promoting effect of type 17 collagen production by chlorogenic acid-loaded PLGA nanoparticles in the human epidermal keratinocyte cell," *Journal of Drug Delivery Science and Technology*, Vol. 58, p. 101624, 2020.

58. Stromberg, Z. R., M. L. Phipps, H. D. Magurudeniya, C. A. Pedersen, T. Rajale, C. J. Sheehan, S. J. Courtney, S. B. Bradfute, P. Hraber, M. N. Rush, J. Z. Kubicek-Sutherland, and J. S. Martinez, "Formulation of stabilizer-free, nontoxic PLGA and elastin-PLGA nanoparticle delivery systems," *International Journal of Pharmaceutics*, Vol. 597, p. 120340, 2021.

59. Halder, K., K. Sabnam, A. Das, D. K. Goswami, and S. Dasgupta, "Thin film formation of HSA in the presence of CTAB-Capped gold nanorods through phase separation," *Langmuir*, Vol. 40, no. 29, pp. 14847–14862, 2024.

60. Betancourt, T., B. Brown, and L. Brannon-Peppas, "Doxorubicin-loaded PLGA nanoparticles by nanoprecipitation: preparation, characterization and in vitro evaluation," *Nanomedicine (London, England)*, Vol. 2, no. 2, pp. 219–232, 2007.

61. Wang, W., D. Song, F. Meng, S. Fan, R. Cai, S. Cheng, C. Shan, T. Xu, H. Zheng, and L. Sun, "Facet-dependent cold welding of au nanorods revealed by liquid cell transmission electron microscopy," *Advanced Science*, Vol. 12, p. 2412779, 2025.

62. Awan, U. A., S. Ali, M. Rehman, N. Zia, S. S. Naz, M. Ovais, and A. Raza, "Stable and reproducible synthesis of gold nanorods for biomedical applications: a comprehensive study," *IET Nanobiotechnology*, Vol. 12, no. 2, pp. 182–190, 2018.